STEREO ANALYSIS OF A SPECIFIC DIGITAL MODEL SAMPLED FROM AERIAL IMAGERY

ARMY ENGINEER TOPOGRAPHIC LABORATORIES,
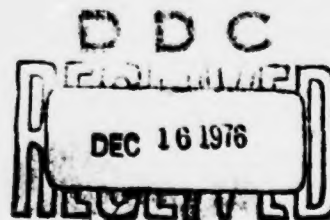FORT BELVOIR, VIRGINIA

SEPTEMBER 1976

363121

STEREO ANALYSIS OF A SPECIFIC DIGITAL
MODEL SAMPLED FROM AERIAL IMAGERY

September 1976

Approved for public release; distribution unlimited.

D D C

DEC 16 1976

F

U.S. ARMY ENGINEER

TOPOGRAPHIC LABORATORIES

FORT BELVOIR, VA 22060

REPORT DOCUMENTATION PAGE		READ INSTRUCTIONS BEFORE COMPLETING FORM
1. REPORT NUMBER ETL-0072	2. GOVT ACCESSION NO.	3. RECIPIENT'S CATALOG NUMBER
4. TITLE *(and Subtitle)* STEREO ANALYSIS OF A SPECIFIC DIGITAL MODEL SAMPLED FROM AERIAL IMAGERY		5. TYPE OF REPORT & PERIOD COVERED Research Note
		6. PERFORMING ORG. REPORT NUMBER
7. AUTHOR(*s*) Michael A. Crombie		8. CONTRACT OR GRANT NUMBER(*s*)
9. PERFORMING ORGANIZATION NAME AND ADDRESS Advanced Technology Division U.S. Army Engineer Topographic Laboratories Fort Belvoir, VA 22060		10. PROGRAM ELEMENT, PROJECT, TASK AREA & WORK UNIT NUMBERS 1T855T20010
11. CONTROLLING OFFICE NAME AND ADDRESS U.S. Army Engineer Topographic Laboratories Fort Belvoir, VA 22060		12. REPORT DATE September 1976
		13. NUMBER OF PAGES 59
14. MONITORING AGENCY NAME & ADDRESS*(if different from Controlling Office)*		15. SECURITY CLASS. *(of this report)* Unclassified
		15a. DECLASSIFICATION/DOWNGRADING SCHEDULE

16. DISTRIBUTION STATEMENT *(of this Report)*

Approved for public release; distribution unlimited.

17. DISTRIBUTION STATEMENT *(of the abstract entered in Block 20, if different from Report)*

18. SUPPLEMENTARY NOTES

19. KEY WORDS *(Continue on reverse side if necessary and identify by block number)*

Correlation	Image Shaping
Array Algebra	Terrain Model
Stereo Matching	Image Warp
Digital Images	Digital Mapping

20. ABSTRACT *(Continue on reverse side if necessary and identify by block number)*

Approximately 160,000 points were matched over a digitized stereo model using correlation algorithms coded in FORTRAN for the CDC 6400. Each of the digitized stereo pair was represented by over 4 million pixels, which were measured on a microdensitometer and stored on disc in the Image Processing Center at ETL. The matched point coordinates and the associated local coordinates were also stored on disc. The derived digital model will be used in the Interactive Image Processing Center to evaluate a variety of problems in digital image processing of stereo photography.

DD $_{1\ JAN\ 73}^{FORM}$ 1473 EDITION OF 1 NOV 65 IS OBSOLETE

i

PREFACE

The work covered by this Research Note was conducted by the Computer Sciences Laboratory (CSL), U.S. Army Engineer Topographic Laboratories (ETL), Fort Belvoir, Virginia. It is part of an effort being carried out in CSL on digital image analysis under Project No. 1T855T20010. Studies were conducted by Michael A. Crombie with computer programming assistance by Thomas A. Hay and Charles A. Haase. Samuel Barr performed the mensuration.

1

CONTENTS

ILLUSTRATIONS

3

TABLES

STEREO ANALYSIS OF A SPECIFIC DIGITAL MODEL SAMPLED FROM AERIAL IMAGERY

INTRODUCTION. The purpose of this report is to describe a stereo matching analysis made at the Computer Sciences Laboratory (CSL), U.S. Army Engineer Topographic Laboratories (ETL). The primary objective was to measure elevation accuracies of heights determined by digitally matching a stereo pair of photographs. This goal could not be met completely in the current effort owing to the lack of imagery with known and photo identifiable ground control. The conventional method of computing a manual estimate of height online was not applicable in this experiment, nor could a set of corresponding points be determined during the image scanning because the PDS I050A microdensitometer is a mono comparator-scanner. The only other method would have been to mark a large number of corresponding points in stereo prior to scanning. However, this procedure would have removed imagery from both images and hampered the matching process. For these reasons, the match results are evaluated in a relative sense. This is done by considering Y-parallax errors, by viewing the shape and numerical values of the correlation, and by reviewing the average signal power and number of successful matches.

A complete analysis of digital matching accuracies for a variety of images and taking geometries is beyond this study. The need for such a study is reviewed in the Discussion section of this report.

However, several secondary objectives were achieved during this study. A controlled digital stereo pair with a dense network of corresponding points is needed at ETL for several in-house studies. The results of this study have provided a stereo scene on disc along with a large number (over 150,000) of matched points at approximately (6-meter) intervals. These data will be used in the interactive digital processing system at ETL to continue a semi-automatic pass point mensuration study, to perform an image warp analysis, and to investigate Fourier matching. The set of data can also be used in a contour analysis or possibly in a controlled feature extraction study.

GEOMETRIC DESCRIPTION. The purpose of this section is to describe the digital images and to determine corresponding points. The various topics in the matching process are enlarged upon in the next two sections.

Scanned Data. The stereo scene is a subset of the stereo model formed by two near vertical images taken on 1 October 1966, near Guadalupe, Arizona. The exterior orientation data is given in a previous ETL Research Note.[1] The upper left corner of the pair was marked in stereo prior to scanning on the PDS 1050A Automatic Microdensitometer System. Eight fiducial marks and their neighboring reseaus along with five reseaus over the approximately 25 -cm square subset were measured

[1] Michael A. Crombie, Philip G. Lem, and Thomas A. Hay, Single Photo Analysis of Sampled Aerial Imagery, U.S. Army Engineer Topographic Laboratories, Fort Belvoir, VA., ETL-RN-74-10, August 1974, AD A012 176.

before and after the scanning process. These data were used to calculate a transformation from pixel space to fiducial space and its inverse.

The images were placed in the microdensitometer comparator so that the base line was parallel to one of the comparator axes. The pixel spacing was 24 μm (Micrometer) and the line spacing was 24 μm. The pixel diameter was 34.5 μm; 2048 lines and 2048 pixels per line were measured on both images. The microdensitometer output 10-bit density data on tape, which was eventually packed and stored on disc in the image processing system at ETL.

Pixel Space and Image Space. Pixel coordinates range from 1 to 2048 for both coordinates (I,J) and for each image. The point at $(1,1)$ on the left image corresponds to the point at $(1,1)$ on the right image because that point was marked in stereo. Note that neither the point at $(1,1)$ nor its immediate neighbors are valid points because of the stereo marking operation. If (I,J) are the pixel coordinates of any point P, then the comparator coordinates are

$$Xpc = Xo - (J-1) * 24$$

$$Ypc = Yo + (I-1) * 24$$

The values (Xo, Yo) are the comparator coordinates of the marked point. Note that the comparator frame is lefthanded and that the Y-axis is toward the flight direction. The fiducial and reseau measurements were used to develop two transformations of the following form:

$$Xpf = r\ Xpc + s\ Ypc + t$$

$$Ypf = u\ Xpc + v\ Ypc + w$$

This transformation is an intermediate one that removes film distortion but does not compensate for radial lens distortion or air refraction. Radial lens distortion was removed by table look up and air refraction distortion was removed by using the simple flat earth model described by Schut.[2] Routines were written for the CDC 6400 to go back and forth between pixel space and image space.

Scene Geometry. The coordinate frames defined above are described in figure 1.

2

 G. H. Schut, "Photogrammetric Refraction" Photogrammetric Engineering, Vol. XXXV, January 1969.
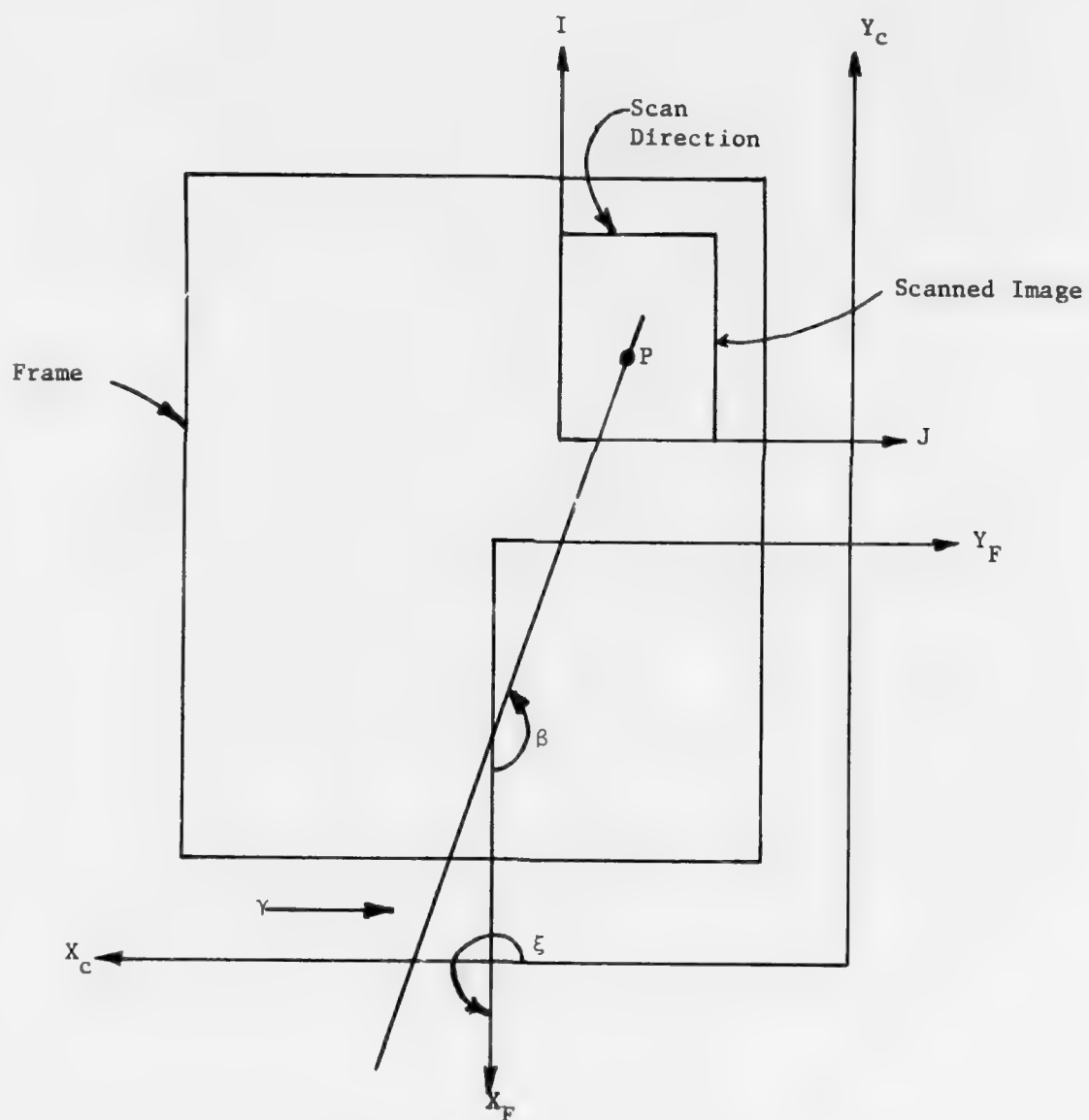
Figure 1. Coordinate Geometry.

7

The symbol γ pertains to the epipolar line through the general point P. If β, exaggerated in the figure, is the epipolar angle of γ with respect to the X_F - axis, then $\pi/2 - (\xi+\beta)$ is the angle γ makes with the Yc and I axes. The angle ξ was estimated from the transformation coefficients to be $\xi \sim \mathrm{Tan}^{-1} (-u/r)$. If the letters L and R pertain to the left and right images, then $\xi L \sim 269.3°$. It can be shown that

$$0.42° \leq \beta L \leq 0.51°$$

$$-0.04° \leq \beta L \leq 0.04°$$

for the image subset; then the epipolar lines γL and γR through corresponding points PL and PR are nearly parallel to the Yc and I axes. This was to be expected, since the photography is near vertical and since the Yc (or I) axis was constrained to be parallel to the base line.

The two images were reproduced on the DICOMED at approximately 1.7x enlargement. The grid on the left (independent) image is defined by the 21 horizontal lines IL and the 21 vertical lines JL.

$$IL = 13 + (N-1) * 100$$

$$JL = 13 + (N-1) * 100$$

$$N = 1, 21$$

The grid is used to define 20 files in the J-direction and 20 blocks in the I-direction. The file and block notation was used as a convenient method for describing areas of interest and for organizing the data reduction. Note that the scan lines (parallel to the J-axis) were moved incrementally in the positive I-direction; whereas, the DICOMED printed the images in the opposite direction.

Matching Procedures. Regular spaced points were defined on the left (independent) image (figure 2), and the match process involved predicting where the corresponding points were on the right (dependent) image (figure 3) and then refining the estimates by using correlation procedures. The match process operated along files processing one block at a time. A modified version of the infiltration method[3] was used to review each match, and the correlation function was developed along the epipolar line through the match point estimate. All matching took place in pixel space. Several aspects of the process are discussed below and in the next two sections.

Prediction and Shaping. Suppose the independent pixel coordinates on the left image are designated (X,Y) and the dependent

[3]Paul Rosenberg, Kent E. Erickson, and Gerhard C. Rowe, Digital Mapping System: Mathematical Processing, U.S. Army Engineer Topographic Laboratories, Fort Belvoir, VA., ETL-CR-74-6, May 1974, AD 782 230.
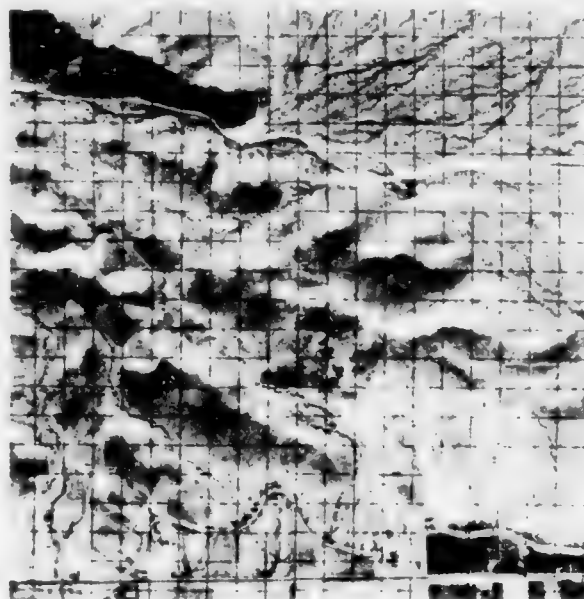
Figure 2. Left Image

Figure 3. Right Image

9

coordinates on the right image are designated (u,v). The (X,Y) values are integer values and were defined for the I block and J file as follows:

$$X_j = X_J + (j-1) * 5$$

$$Y_i = Y_I + (i-1) * 5$$

i and j range from 1 to 20.

$$X_J = 16 + (J-1) * 100$$

$$Y_I = 16 + (I-1) * 100$$

J = 1, 20 files

I = 1, 20 blocks

Thus, 400 points are defined in each of the 400 blocks.

It is assumed that one-to-one transformations u=u (X,Y) and v=v (X,Y) exist and that the Taylor expansions, up to but not including second order terms, are close approximations to the transformations over small regions. Suppose that (Xp, Yp) and (up, vp) are corresponding points, then

$$up' \sim up + \frac{\delta u}{\delta X} \Delta X + \frac{\delta u}{\delta Y} \Delta Y$$

$$vp' \sim vp + \frac{\delta v}{\delta X} \Delta X + \frac{\delta v}{\delta Y} \Delta Y$$

where

$$Xp' = Xp + \Delta X$$

$$Yp' = Yp + \Delta Y$$

The up' and vp' equations are the estimators. The independent increments ΔX and ΔY are defined in a regular fashion, and the partial derivatives are estimated from neighboring matches.

A point is redefined as an array of pixels centered over the point for the correlation calculations. The left array is shaped, since a number of arrays must be defined on the right image in order to develop the correlation function. The spacing in the left array is

10

$$\begin{pmatrix} \Delta x \\ \Delta y \end{pmatrix} \sim \begin{pmatrix} \dfrac{\delta u}{\delta X} & \dfrac{\delta u}{\delta Y} \\[2mm] \dfrac{\delta v}{\delta X} & \dfrac{\delta v}{\delta Y} \end{pmatrix}^{-1} \begin{pmatrix} \Delta u \\ \Delta v \end{pmatrix}$$

where in this instance $\Delta u = \Delta v = 1$, i.e. uniformly spaced pixels on the right image are used. It is still necessary to resample for gray shades on the right image, but the number of computer multiplies is diminished.

Modified Infiltration. The infiltration method is a relatively complex process that follows the path of easiest correlation. That is, the process results dictate the direction of the process, and the system evaluates each match to determine whether it is acceptable or not. Thus, regions of low signal power are avoided until surrounding regions of better imagery are matched. The more difficult regions are then processed utilizing all of the acquired parallax information or else are avoided completely. In this manner, the system matches all of the model that can be matched, and in the process delineates those regions that cannot be matched, e.g. ponds, clouded areas, occluded areas. The infiltration method was demonstrated for small scenes in a previous ETL report.[4] A need exists for a special computing capability and for large amounts of readily accessible computer storage before the process can be used over an entire model or even over 10 percent of one as in this exercise. For this reason, the following procedure was tested.

The independent points for the blocks are shown in figure 4. The last two rows of matched results from the previous block and the last two columns of matched results of the same block from the previous file were used to begin processing the current block. These data along with matched results of this block were used to compute the partial derivative estimates used for predicting and shaping. The matching process (explained below) produced a numerical evaluation of each match. At the completion of the block run, each of the 400 matches was compared to a predetermined criterion. Those points that failed were rematched, this time using a larger defining array of pixels and a more refined partial derivative estimate.

Evaluation. Since the defining epipolar plane through the base line and the independent point (X,Y) is known, the epipolar line on the dependent image can be easily computed. A correlation function through the dependent coordinate estimate (up', vp') and parallel to the epipolar line is generated. A second correlation function through the estimate and perpendicular to the epipolar line is also computed. Note that the slope of the epipolar line changes very slowly over the model subset.

[4]Paul Rosenberg, Kent E. Erickson, and Gerhard C. Rowe, Digital Mapping System: Mathematical Processing, U.S. Army Engineer Topographic Laboratories, Fort Belvoir, VA., ETL-CR-74-6, May 1974, AD 782 230.
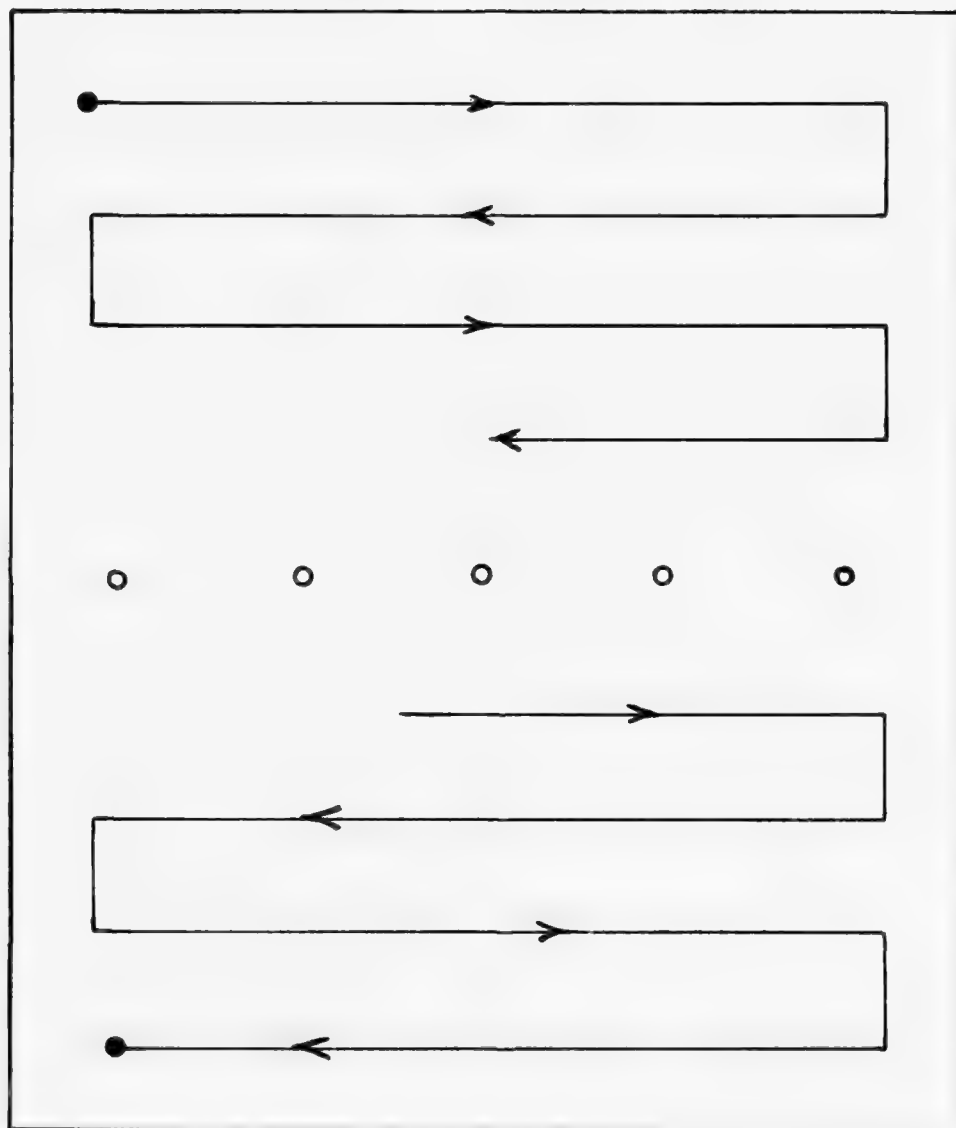
Figure 4. Independent Point Path.

12

The shift along the epipolar line corresponding to the peak correlation is used to refine the estimate. The shift perpendicular to the epipolar line is also estimated, and a fraction of this shift is applied to the estimate as a means for controlling Y-parallax error build-up. Y-parallax is a photogrammetric term for the component of missmatch normal to the epipolar line. The term is used exactly in that context in this report even though the pixel Y-direction is nearly parallel to the epipolar direction. Thus, Y-parallax errors in this exercise are actually in the X-direction.

A quadratic function was fit through the largest of the discrete correlation values and its adjacent neighbors. The shape of the correlation curve was used to evaluate the match. A narrow correlation function is regarded as indicative of a better match than a flatter one. For this reason, the product of the second derivatives of the two functions was used to evaluate the match. Large positive values of the product indicate successful matches.

The numerical correlation procedure is shown in figure 5.
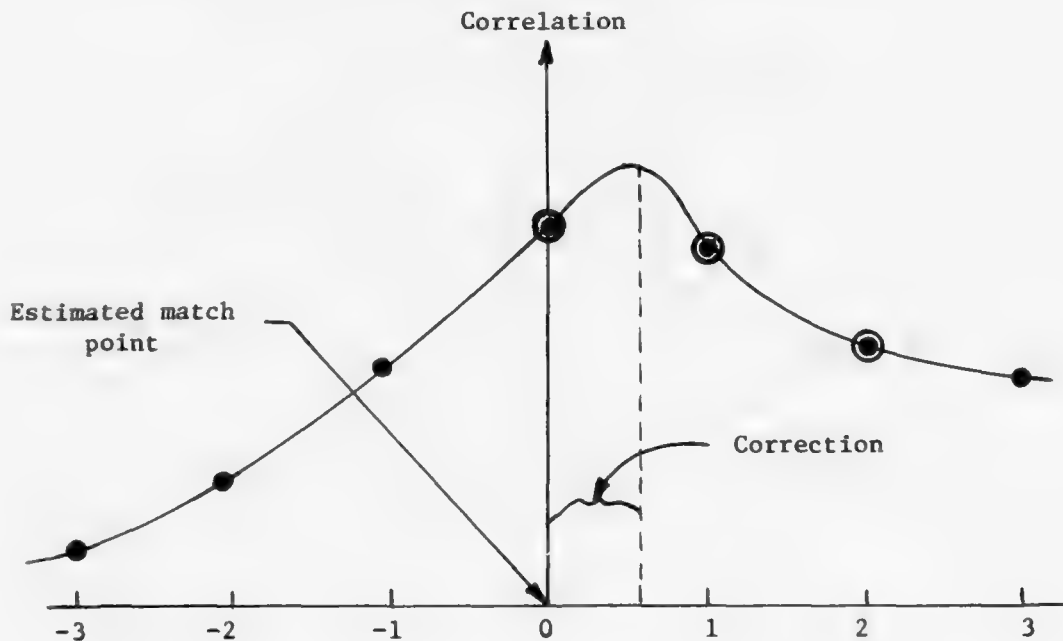
Figure 5. Correlation Function.

13

In this example, the encircled discrete correlation values would be used
to estimate the function, the shift, and finally the shape of the corre-
lation function. The individual correlation value used in this exercise
was the linear correlation coefficients of statistics.

$$R_{lr} = \frac{\Sigma (1 - \bar{1}) (r - \bar{r})}{[\Sigma (1 - \bar{1})^2 \Sigma (r - \bar{r})^2] \frac{1}{2}}$$

The summation is taken over the defining array where 1 and r pertain to
the gray shades of the left and right images, respectively.

Geometric Control. Several techniques were used to maintain
geometric control over the process. One technique was described above
in the section on the Modified Infiltration method. Continuity was
maintained over blocks and files by using boundary data of previously
matched blocks to help compute the partial derivatives needed for depen-
dent coordinate estimating and shaping. Modifications to the general
technique were needed for File #1 and for all 20 of the first blocks.

In order to maintain continuity within a block, a five-point cubic
smoothing function was applied to each of the 20 lines after they were
matched. The last two points of the adjacent block were included in the
smoothing. At the completion of the block run, 25 points were inter-
sected in object space to determine if a significant amount of Y-parallax
had crept into the computations. If the Y-parallax estimate exceeded a
a test criterion (5µm in this exercise), then each of the 400 points were
corrected. This was done by allowing all of the intersection error to be
taken up by the dependent coordinates in image space. The reason for this
is that the independent coordinates are correct by definition. The
derived transformation from image space to pixel space was applied to the
image space corrections to derive the appropriate dependent pixel space
corrections.

NUMERICAL EXPERIMENT. The purpose of this section is to describe
some of the preliminary tests and operations that were performed on the
digital image pair and also to describe the results of the final computer
run. Matching parameters determined in the preliminary tests were used to
specify the matching procedure of the final computer run.

Preliminary Tests. Prior to matching a large number of
corresponding points over the digital model, two series of tests were
performed. The first series were analytical tests that utilized the
geometry of the imagery to obtain bounds on the shape parameters and on
the expected parallax changes. The second series were numerical tests
designed to evaluate the analytical results and to compute practical
matching parameters.

Analytical. Scale change determination for image segments along

14

epipolar lines for changing slopes is critical to correct image shaping and to estimate precise match points. The estimate of the match points must be as accurate as possible so as to reduce the dimension of the correlation function in the refinement process. One purpose of this analysis was to compute reasonable upper and lower bounds of the stretch parameter so that the sample estimate could be constrained. It was expected that the matched data would be subject to noise, which is magnified in the process of computing sample derivatives. The equation used to compute the results below is contained in appendix A.

The scale change parameter is the ratio of corresponding image segments for a particular ground segment. Since the shape parameter decreases as the location parameters ω and ξ (see appendix A) increase, table 1 pertains to $\xi = \omega = 0$. The table pertains to slopes at the nadir of the first image and to a base-height ratio of $B/H = 0.6$.

α	S
0	1.000
5	1.055
10	1.118
15	1.192
20	1.279
25	1.389
30	1.530
35	1.725
40	2.014
45	2.500

Table 1. Maximum Scale Change Parameters

The angle α is expressed in degrees and is the slope of the terrain in object space. Note that the results pertain to a segment tilted toward image 2. If the slope is in the opposite direction, then S is the reciprocal of the values given above. If the slope is less than 25° in absolute value, then $0.7 \leq S \leq 1.4$. In the section on Scene Geometry above, the angle between the epipolar line and the Y-axis was less than one degree. For this reason, $\frac{\delta V}{\delta Y} = V_Y$ was constrained to lie between 1.4 and 0.7. In order to account for nonlinearity in the scanner and differences between the ideal and the actual, the following constraints were also applied:

$$0.995 \leq \frac{\delta U}{\delta X} = U_X \leq 1.005$$

$$-0.005 \leq \frac{\delta U}{\delta Y} = U_Y \leq 0.005$$

$$-0.005 \leq \frac{\delta V}{\delta X} = V_X \leq 0.005$$

Control was maintained on any one of the four shape parameters (say W) in two ways:

        1.   Compute running average
        2.   Enforce constraints

The running average is simply

$$W_{I+1} = \beta * W_I + (1-\beta) * W_o$$

where

W_{I+1} : updated value

W_I : previous value

W_o : sample value

β : running average weight; $o \leq \beta \leq 1$

This calculation only applies if the sample value was computed in the immediate neighborhood of the previous value. The updated value is constrained to lie within the boundaries given above.

For a variety of reasons, such as inadequate shaping, poor match point estimation, lack of image detail, occluded scenes, it is very possible that the process could lock onto the wrong point especially when the matching arrays are small. Thus, reasonable bounds must be placed on the parallax corrections that are directly related to changes in terrain slope. Table 2 presents expected pixel shifts as a function of slope change $\Delta\alpha$ and pixel spacing M. The entries pertain only to the digital image model analyzed in this exercise.

It was assumed in the derivation of table 2 that the terrain had been flat when an abrupt change of $\Delta\alpha$ occurred. The entries in table 3 are multiplicative scale factors that can be used to increase the expected parallax shifts of table 2 whenever the original slope was α. It is evident that any pixel shift larger than one spot should be suspect.

Numerical. The initial computation was a fishing expedition to determine a starting point for subsequent computations. The pixel located at JX = IY = 16 on the left image was chosen arbitrarily, and a coarse matching procedure was initiated at and around UJ = VI = 16.0 on the right image. A two-dimensional correlation function was generated by allowing VI to vary in increments of one pixel from VI = 11.0 and continuing until VI = 40.0. Since the I-axis is nearly parallel to the

Table 2.   Parallax Shift Due to Slope Changes.

M $\overset{\Delta\alpha}{\diagdown}$	5°	10°	15°	20°	25°
1	.01	.03	.04	.05	.07
2	.03	.05	.08	.11	.14
3	.04	.08	.12	.16	.21
4	.05	.11	.16	.22	.28
5	.07	.13	.20	.27	.35
6	.08	.16	.24	.33	.42
7	.09	.19	.28	.38	.49
8	.10	.21	.32	.44	.56
9	.12	.24	.36	.49	.63
10	.13	.26	.40	.54	.70

Table 3.   Parallax Shift Scale Factors.

$\Delta\alpha \overset{\alpha}{\diagdown}$	5°	10°	15°	20°	25°
5°	1.02	1.03	1.10	1.17	1.27
10°	1.02	1.06	1.12	1.21	1.33
15°	1.03	1.08	1.15	1.25	1.39
20°	1.04	1.10	1.19	1.31	1.47
25°	1.05	1.12	1.22	1.36	1.56

epipolar direction, UJ was allowed to vary in increments of one pixel
from UJ = 14.0 to UJ = 18.0.   There was no shaping, the linear corre-
lation coefficient was used, and the array size was 21 x 21.   The peak
correlation was determined by inspection from the 150 correlation values
to be located at UJ = 16.0 and VI = 32.0.   Thus, the following
coordinate pair in pixel space were regarded as good starting values in
subsequent computer runs:

Left Image	Right Image
JX = 16	UJ = 16.0
IY = 16	VI = 32.0

A variety of computer runs were performed over Block 1 (B1) of File
1 (F1) as a means to get reasonable parameters for the subsequent pro-
cessing of the digital model.   The process described in figure 4 could
not be used, since the required starting data did not exist.   The first
step was to match the four points in figure 6.
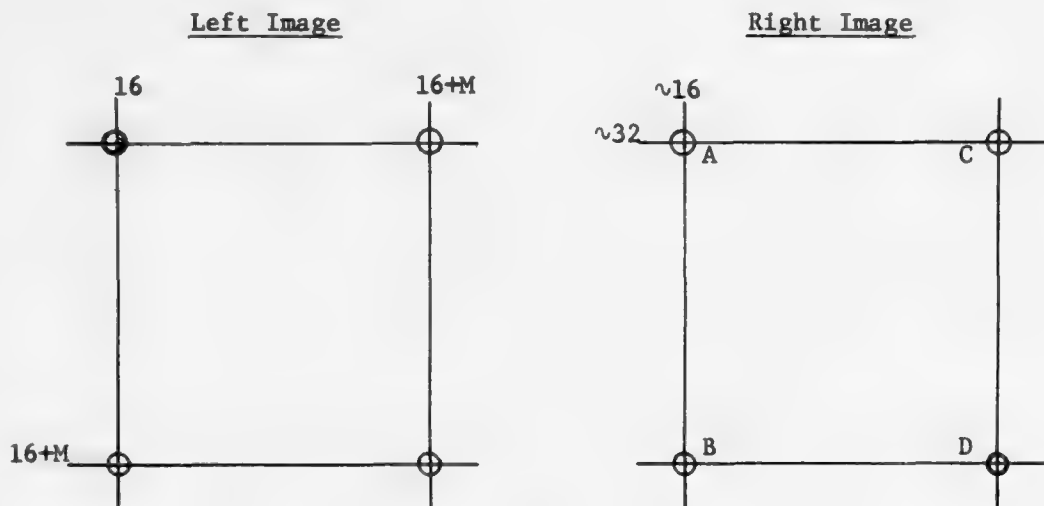
Figure 6. Initial Pattern.

The output pixel spacing M on the left image was one of the parameters
that was varied. The corresponding points on the right image were
estimated by assuming zero parallax. For example, after point A was
refined, the coordinates of point B were estimated to be

$$UJ_B = UJ_A$$

$$VI_B = VI_A + M$$

The refinement process consisted of developing LC correlation values along
the epipolar line through the estimate and also LC correlation values
normal to the epipolar line and of then correcting the estimate by the
shift as described in figure 5. The number of correlation values LC, the
form of the correlation measure, the array size, and the resampling
procedure along with the output spacing M are some of the parameters that
were analyzed in the preliminary tests.

Twenty rows and twenty columns of matched points were processed in
the several preliminary tests. The remaining 396 points were matched
over the pattern in figure 7.
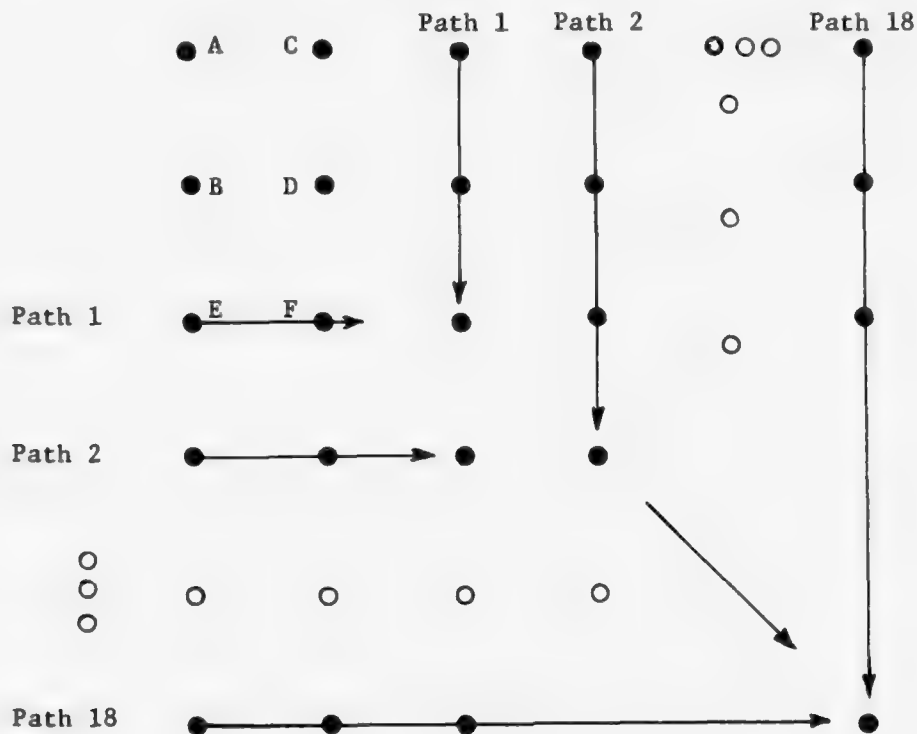
Figure 7.   Preliminary Test Point Path.

Local parallax information was used for both predicting and array shaping.
For example, the partial derivatives for points E and F were computed
from the following equations:

$$\frac{\delta U}{\delta X} = \frac{1}{2M} \ (U_C - U_A + U_D - U_B)$$

$$\frac{\delta U}{\delta Y} = \frac{1}{2M} \ (V_C - V_A + V_D - V_B)$$

$$\frac{\delta V}{\delta X} = \frac{1}{2M} \ (U_B - U_A + U_D - U_C)$$

$$\frac{\delta V}{\delta Y} = \frac{1}{2M} \ (V_B - V_A + V_D - V_C)$$

The shape parameter estimates were more complicated as the point in question moved away from the boundary. Also, the running average notion and the constraints described above were utilized.

The objective of the preliminary numerical tests was to determine a sensible set of match parameters for the digital imagery used in this experiment. It appears that such a study is required whenever new imagery is tested. The following parameters were evaluated for the initial tests on B1 of F1:

IC : Array Size
LC : Length of Correlation Function
 M : Output Spacing
RES: Resampling Method
CM : Correlation Measure
YP : Y-Parallax Correction

The specific goals were to minimize IC and LC, to maximize M, and to simplify RES, CM, and YP. One restraint on the matching procedure was that the digital data was stored on disc, had to be extracted from disc memory, and put into core memory before processing. The parameter selection was tempered by the limits on core memory, and the time required to transfer data between disc memory and core.

The array size IC was varied from 7 to 19 pixels, and the length of the correlation function LC was varied from 5 to 9 pixels. The output spacing M was varied from 1 to 5 pixels. The two correlation measures RXY and SXY were compared, and the bilinear interpolation and nearest neighbor resampling procedures were compared. The RXY and SXY measures are defined as

$$RXY = \sigma_{xy}/\sigma_x\sigma_y$$

$$SXY = \sigma_{xy}$$

The symbols σ_{xy}, and σ_x, and σ_y are the covariance of X and Y, the standard deviation of X, and the standard deviation of Y, respectively. The two arrays of pixels are symbolized as X and Y. Finally, the Y-parallax correction was evaluated at $\epsilon=0.01$, 0.05 and 0.1 times the computed shift in the direction normal to the epipolar direction.

There were 400 matches for each of the approximately 20 computer runs. An extensive correlation history was printed out for each match. The output included the correlation function values, the estimated X-parallax shifts, the shape parameters, signal power, confidence measure, and finally the Y-parallax error for each of the matching paths described in figure 7. The two basic measures of effectiveness were the Y-parallax errors and the computed X-parallax shifts. The X-parallax shifts were compared to table 2. X-parallax is a photogrammetric term for the component of missmatch along the epipolar

20

direction. Thus, X-parallax errors in this exercise are actually in the pixel Y-direction.

The tightest control on Y-parallax ($\varepsilon=0.01$) produced the best results. The primary reason for this is that the epipolar directions were known accurately. However, Y-parallax must still be controlled for two reasons. First, the inaccuracies in the prediction parameters will cause errors in Y-parallax. Second, nonlinearities in the scanner will also cause Y-parallax errors.

Several general observations were made as the output spacing M and the array size IC were varied.

1. The match results, except for M = 1, generally improved as IC increased.

2. The match results definitely worsened for M = 1 as IC increased.

3. Except for IC = 7, results generally improved as M increased.

4. The match results definitely worsened for IC = 7 as M increased.

5. Although there was an improvement in output quality as IC increased from 11 to 19 for M > 1, the results were not nearly as significant as the change from IC = 7 to IC = 11.

6. The match results, except for M = 1, definitely worsened for IC = 7 as the length of the matching path increased.

The first two observations indicate that when the spacing M is small with respect to the array size IC, then first order shaping can easily produce incorrect results. This is true because the computed shape parameters pertain to a small percentage of the array. As M increases with respect to IC, the estimated shape parameter is more nearly the average of the array.

The third and fourth observations indicate that when the spacing is large with respect to the array size, then again first order shaping can easily produce incorrect results. Again, this is true because the estimated shape parameter pertains to only a small percentage of the array. For example if M = 5 and IC = 7, then no portion of the previously estimated match points used to update the shape parameters are i ..uded in the central array. When M = 5 and IC = 11, the central just barely overlaps the previously matched data.

The four observations taken together are not contradictory. They indicate, for the parameter range considered in the tests, that there

21

is an optimal set somewhere between the extremes. The output spacing M = 5 was chosen to reduce the computation time and to reduce the amount of storage. The array size was set to IC = 11 because of the fifth observation. In order to take advantage of the improvement in output as IC is increased, IC was set to 19 for the rematch procedure described in the section on Modified Infiltration.

The sixth observation indicates that if an inappropriate set of matching parameters are chosen, then the errors are likely to propagate unfavorably. It would be very uncertain to rely on correlation methods to recover lost correlation, unless a strategy is developed to do so.

From tables 2 and 3 and for M = 5, the largest computed shift along the epipolar line owing to a change in ground slope should be less than 0.6 pixel. Since the shape and prediction parameters are estimated and therefore contain errors, the computed pixel shift can be as large as one pixel spacing and even a bit larger when traversing steep areas of low contrast. For these reasons, the number of correlation values LC should not exceed 5, i.e. two values on either side of the estimate. In fact, the match results definitely got worse as LC increased from 5 to 9.

It was shown in an ETL Research Report[5] that the linear correlation coefficient RXY is superior to the covariance SXY in stereo image matching. It was shown again in this preliminary numerical analysis that RXY is indeed superior to SXY, especially in areas of low contrast. Finally, there was a significant improvement in match quality when the pixels of the shaped arrays were determined by interpolation rather than by nearest neighbor. Although RXY generally takes twice the compute time of SXY and interpolation takes longer to compute than nearest neighbor, it was felt that the increase in compute time was well worth the effort since fewer strategies would be needed in steep areas and or in areas of low contrast.

Stereo Processing of the Stereo Image Pair. The digital imagery was processed one file at a time. The first block (B1) of each file was processed first by tying it to B1 of the previous file. The tie was implemented by using the last two columns of results of the prior block for developing of shape parameters, for predicting, and for smoothing. The remaining blocks in the file were processed sequentially; wherein, the last two columns of the corresponding block in the previous file and the last two rows of the prior block in the current file were used to maintain continuity. The first block of the first file (F1) was processed independently of the neighboring blocks. The remaining blocks

[5]Michael A. Crombie, Semi-Automatic Pass Point Determination Using Digital Techniques, U.S. Army Engineer Topographic Laboratories, Fort Belvoir, VA., ETL-0051, December 1975, AD A026 082.

of F1 were processed sequentially; wherein, the last two rows of results from the previous block were used to maintain continuity.

An attempt to match the 400 output points of each block was made in Mode 1 of the operation. Those points not meeting the success criterion were rematched in Mode 2. If, during Mode 1, the confidence measure $C\phi N \geq 0.01$, then the match was judged to be a success; $C\phi N$ is the product of the two second derivatives of the two correlation functions associated with each match. The array size in Mode 1 was IC = 11 and in Mode 2 it was IC = 19. The following set of parameters was used in the match process:

Length of Correlation Function: LC = 5 pixels
Output Spacing   : M = 5 pixels
Correlation Measure   : RXY
Y-Parallax Correction   : $\epsilon = 0.01$
Running Average Weight   : $\beta = 0.50$
Y-Parallax Criterion   : $\delta = 5 \ \mu m$

If the sample estimate of the Y-parallax error exceeded δ, then all 400 points were corrected for Y-parallax. The bilinear interpolation for gray shades was used in the resampling operation, and the shape parameters were constrained by the following bounds:

$$0.995 \leq U_X \leq 1.005$$

$$-0.005 \leq V_X \leq 0.005$$

$$-0.005 \leq U_Y \leq 0.005$$

$$0.700 \leq V_Y \leq 1.400$$

Numerical Results. The computer program was organized so that only enough pixel data was extracted from disc to process one block at a time. The pixel data dimension of the independent image subset was constant for each block. The pixel data from the dependent image varied over blocks owing to the undulating terrain. The initial line of pixel data on disc for the dependent image was estimated accurately by reviewing the dependent coordinates of the last line of output data from the previous block.

Not all of the first blocks could be matched in their entirety, since the dependent pixel data did not extend for enough in the minus Y-direction beginning approximately at F3. Line 10 of B1 for all 20 files was the first completely matched line. Thus, there are 400 * 391 = 156,400 matched points over the digital model.

The basic outputs from the process are the dependent pixel coordinates on the second image associated with the regularly spaced inde-

23

pendent coordinates on the first image. These results were stored on disc into two (400 x 400) regions. If the independent pixel coordinates on the first image are defined to be

$$X = 16 + (J-1) * 5$$

$$Y = 16 + (I-1) * 5$$

$$I = 10,400 \text{ and } J = 1,400$$

then the dependent pixel coordinates on the second image are stored on disc in

$$U = DEPX \ (I,J)$$

$$V = DEPY \ (I,J)$$

where

DEPX and DEPY are the areas on disc reserved for the dependent data.

Thus, the 156,400 corresponding pairs of points are defined by (I,J) in the first case and located on disc by (I,J) in the second case.

The origin of a local rectangular coordinate frame was located at pixel coordinates $X_\phi = Y_\phi = 1011$ of the independent image. The corresponding pixel coordinates on the dependent image are located at $U_\phi = DEPX \ (200,000)$ and $V_\phi = DEPY \ (200,000)$. These data were transferred to image space, corrected for distortion, and then intersected in the earth fixed geocentric reference frame. The geocentric coordinates of the origin were used to establish a local coordinate frame; wherein, the $X_L Y_L$-plane is tangent to the Clarke 1866 spheroid at the nadir of the intersected point and where the X_L-axis is toward the north. Finally, the remaining 156,399 points were intersected in the local frame, and the resulting rectangular coordinates were stored in three areas on the same disc as (U,V). The local coordinates were stored in

$$X_L = XX \ (I,J)$$

$$X_L = YY \ (I,J)$$

$$Z_L = ZZ \ (I,J)$$

The results of the match exercise are characterized numerically by the four tables given below. The results are enlarged upon in the Discussion section. The computer program was designed to produce the average correlation, the average signal power, and the average confidence measure for each block. The average correlation for a block is defined to be:

24

Table 4. Average Correlation Values

FILE NUMBER

1	2	3	4	5	6	7	8	9	10
.772	.743	.614	.567	.573	.457	.440	.503	.562	.504
.705	.757	.726	.704	.671	.621	.636	.597	.690	.676
.782	.745	.684	.690	.745	.732	.647	.637	.685	.746
.831	.807	.784	.750	.823	.832	.752	.741	.798	.746
.774	.770	.832	.725	.740	.757	.859	.888	.869	.855
.740	.779	.791	.828	.775	.792	.793	.828	.743	.783
.675	.697	.767	.810	.779	.801	.736	.758	.754	.811
.589	.610	.775	.807	.772	.776	.754	.788	.749	.725
.731	.547	.626	.639	.803	.757	.690	.624	.621	.687
.616	.622	.608	.669	.593	.783	.692	.710	.714	.742
.735	.589	.584	.558	.631	.757	.732	.725	.734	.736
.702	.618	.482	.663	.536	.520	.657	.762	.721	.722
.730	.653	.496	.626	.479	.565	.485	.487	.766	.787
.769	.632	.496	.719	.474	.594	.584	.565	.667	.740
.669	.604	.543	.623	.510	.692	.565	.596	.642	.677
.583	.563	.517	.636	.567	.630	.688	.502	.653	.686
.555	.657	.550	.596	.678	.592	.607	.713	.687	.824
.615	.672	.566	.567	.741	.754	.685	.722	.797	.738
.652	.628	.476	.493	.767	.781	.784	.482	.533	.720
.785	.734	.687	.772	.830	.657	.736	.619	.659	.713

Table 4. (Cont'd)

FILE NUMBER

11	12	16	14	15	16	17	18	19	20
.572	.513	.556	.529	.530	.622	.576	.622	.586	.614
.693	.715	.764	.740	.804	.757	.802	.805	.817	.713
.700	.707	.814	.801	.704	.728	.765	.773	.788	.754
.729	.712	.730	.700	.733	.763	.790	.770	.719	.683
.778	.785	.751	.681	.753	.776	.794	.722	.719	.759
.851	.749	.815	.836	.844	.814	.790	.794	.770	.805
.748	.588	.657	.820	.718	.653	.713	.720	.793	.748
.560	.522	.514	.568	.505	.637	.605	.681	.718	.808
.649	.695	.523	.646	.659	.674	.695	.580	.708	.781
.619	.746	.621	.607	.664	.702	.657	.671	.752	.759
.696	.759	.708	.718	.676	.692	.701	.706	.709	.768
.753	.831	.754	.759	.693	.656	.740	.708	.573	.662
.761	.743	.789	.725	.751	.708	.775	.738	.675	.675
.737	.627	.707	.722	.684	.585	.633	.681	.670	.539
.655	.724	.632	.710	.692	.675	.658	.689	.683	.635
.622	.519	.721	.700	.758	.738	.622	.596	.631	.631
.545	.565	.641	.547	.583	.781	.558	.539	.600	.533
.714	.719	.517	.590	.739	.737	.702	.695	.570	.594
.603	.691	.726	.693	.593	.681	.666	.712	.739	.730
.660	.575	.615	.689	.546	.340	.257	.363	.397	.503

Table 5. Average Signal Power

FILE NUMBER

1	2	3	4	5	6	7	8	9	10
310.	305.	299.	200.	193.	192.	224.	276.	272.	214.
225.	305.	287.	309.	230.	202.	200.	193.	227.	199.
274.	267.	273.	251.	277.	289.	211.	195.	209.	216.
330.	315.	334.	347.	399.	415.	308.	311.	271.	233.
231.	255.	283.	245.	220.	271.	368.	399.	328.	350.
211.	235.	270.	297.	237.	264.	273.	315.	261.	271.
195.	242.	220.	247.	250.	283.	229.	264.	302.	330.
193.	165.	248.	265.	227.	215.	253.	292.	288.	231.
221.	202.	204.	178.	255.	232.	172.	157.	138.	204.
172.	205.	187.	168.	151.	253.	199.	252.	199.	214.
247.	197.	202.	171.	177.	255.	210.	245.	243.	259.
215.	233.	158.	213.	154.	159.	225.	253.	229.	207.
246.	25..	185.	225.	162.	195.	143.	138.	297.	308.
256.	282.	201.	256.	201.	212.	216.	178.	198.	274.
225.	290.	217.	196.	213.	261.	201.	204.	211.	218.
192.	269.	243.	220.	200.	221.	249.	195.	233.	246.
207.	355.	307.	194.	234.	194.	214.	265.	284.	420.
222.	325.	246.	193.	281.	391.	344.	312.	400.	289.
266.	348.	232.	202.	368.	331.	307.	188.	165.	278.
376.	354.	311.	361.	483.	291.	329.	254.	261.	313.

27

Table 5. (Cont'd)

FILE NUMBER

11	12	13	14	15	16	17	18	19	20
241.	227.	266.	260.	271.	383.	279.	286.	301.	300.
214.	225.	281.	264.	339.	274.	309.	323.	339.	257.
221.	275.	348.	335.	235.	252.	298.	307.	293.	251.
226.	219.	238.	255.	264.	258.	295.	283.	225.	267.
256.	244.	271.	221.	269.	287.	271.	214.	258.	266.
340.	252.	308.	311.	331.	291.	260.	247.	262.	304.
321.	200.	247.	339.	253.	184.	227.	250.	285.	236.
189.	164.	167.	139.	163.	213.	201.	220.	229.	268.
267.	231.	158.	196.	188.	208.	245.	234.	216.	240.
258.	243.	184.	186.	212.	214.	217.	270.	261.	235.
232.	257.	235.	242.	218.	203.	235.	237.	250.	269.
263.	301.	257.	251.	220.	225.	257.	212.	186.	220.
280.	297.	262.	237.	259.	232.	270.	270.	240.	235.
291.	222.	217.	260.	209.	170.	204.	264.	233.	204.
234.	305.	181.	258.	270.	224.	225.	232.	242.	230.
225.	174.	285.	222.	272.	259.	342.	274.	272.	232.
195.	283.	242.	231.	169.	297.	223.	177.	257.	198.
307.	290.	195.	213.	377.	307.	327.	342.	243.	256.
271.	347.	392.	423.	372.	450.	503.	550.	447.	464.
265.	245.	251.	323.	437.	481.	505.	383.	420.	467.

Table 6. Average Confidence

FILE NUMBER

1	2	3	4	5	6	7	8	9	10
.064	.040	.016	.074	.030	.028	.032	.034	.054	.028
.072	.063	.051	.029	.035	.033	.049	.039	.050	.051
.046	.053	.044	.057	.073	.051	.041	.031	.045	.048
.037	.044	.040	.033	.041	.048	.052	.048	.044	.049
.047	.046	.053	.037	.033	.031	.043	.036	.034	.057
.039	.042	.038	.034	.043	.038	.039	.034	.035	.046
.027	.028	.034	.033	.041	.037	.034	.033	.033	.032
.032	.021	.033	.025	.034	.038	.031	.030	.029	.023
.033	.018	.024	.023	.042	.041	.030	.031	.026	.030
.045	.044	.032	.020	.030	.035	.035	.040	.040	.036
.039	.038	.034	.038	.032	.034	.033	.044	.052	.038
.045	.033	.031	.036	.031	.022	.035	.039	.041	.049
.049	.036	.030	.031	.026	.029	.031	.031	.039	.045
.047	.035	.042	.041	.039	.057	.056	.044	.036	.036
.047	.036	.044	.053	.037	.060	.063	.081	.068	.038
.050	.037	.042	.063	.057	.046	.066	.041	.061	.057
.034	.026	.026	.058	.069	.051	.041	.051	.050	.045
.023	.029	.030	.035	.039	.040	.043	.037	.040	.055
.024	.026	.022	.023	.031	.045	.046	.026	.024	.041
.024	.025	.022	.023	.026	.025	.033	.023	.017	.025

29

Table 6. (Cont'd)

FILE NUMBER

11	12	16	14	15	16	17	18	19	20
.042	.033	.033	.045	.061	.068	.092	.093	.080	.056
.053	.053	.066	.060	.072	.087	.102	.097	.107	.065
.045	.039	.043	.069	.066	.056	.072	.086	.082	.072
.051	.059	.044	.051	.058	.082	.100	.082	.074	.071
.045	.046	.039	.047	.050	.061	.065	.080	.066	.067
.049	.029	.022	.032	.039	.061	.045	.053	.043	.044
.025	.026	.032	.030	.043	.033	.045	.048	.039	.068
.021	.017	.024	.033	.020	.027	.027	.039	.045	.041
.025	.034	.024	.033	.029	.029	.039	.037	.050	.075
.022	.038	.039	.039	.040	.037	.039	.040	.047	.057
.030	.036	.038	.043	.033	.033	.040	.048	.047	.039
.036	.043	.039	.043	.036	.041	.035	.026	.021	.038
.051	.035	.051	.054	.050	.048	.049	.034	.028	.047
.036	.038	.048	.047	.031	.037	.030	.055	.044	.034
.047	.039	.034	.045	.041	.031	.026	.043	.044	.046
.053	.039	.038	.039	.030	.045	.013	.023	.039	.053
.037	.033	.030	.019	.014	.026	.042	.054	.045	.039
.043	.041	.029	.026	.017	.018	.033	.054	.051	.042
.029	.030	.026	.023	.019	.074	.034	.021	.038	.039
.017	.016	.014	.016	.017	.024	.009	.016	.020	.025

Table 7. Total Successful Matches

FILE NUMBER

1	2	3	4	5	6	7	8	9	10
350.	297.	179.	276.	277.	268.	259.	278.	278.	274.
400.	389.	364.	283.	284.	327.	375.	386.	392.	389.
388.	394.	364.	391.	400.	372.	346.	339.	393.	380.
380.	357.	390.	351.	319.	385.	399.	385.	353.	382.
379.	393.	385.	345.	361.	353.	380.	322.	323.	369.
369.	382.	382.	374.	390.	358.	351.	358.	364.	382.
331.	319.	352.	370.	392.	372.	350.	325.	307.	336.
322.	258.	360.	330.	348.	360.	359.	363.	333.	304.
338.	240.	321.	286.	380.	383.	339.	362.	327.	319.
365.	324.	304.	242.	326.	373.	367.	356.	370.	379.
385.	366.	343.	364.	343.	355.	372.	380.	396.	373.
376.	343.	312.	379.	332.	269.	369.	374.	385.	397.
394.	330.	308.	355.	284.	289.	302.	329.	363.	390.
393.	306.	303.	384.	315.	392.	392.	362.	386.	373.
389.	302.	298.	387.	315.	383.	396.	399.	382.	370.
376.	317.	290.	394.	358.	386.	392.	324.	397.	375.
327.	287.	277.	390.	391.	385.	371.	386.	385.	387.
251.	279.	260.	351.	371.	368.	362.	375	373.	385.
234.	242.	227.	258.	333.	365.	356.	315.	290.	373.
285.	265.	249.	293.	299.	300.	323.	285.	226.	265.

31

Table 7.   (Cont'd)

FILE NUMBER

11	12	16	14	15	16	17	18	19	20
283.	294.	262.	283.	291.	300.	319.	297.	298.	292.
390.	396.	393.	388.	390.	398.	400.	400.	400.	394.
393.	335.	381.	393.	393.	395.	397.	400.	398.	400.
390.	387.	384.	374.	389.	369.	400.	400.	400.	377.
374.	375.	377.	369.	389.	394.	400.	400.	394.	391.
371.	226.	257.	312.	360.	393.	385.	396.	351.	317.
309.	298.	334.	335.	360.	357.	378.	368.	391.	394.
259.	212.	280.	345.	243.	310.	298.	319.	348.	356.
291.	359.	256.	325.	293.	341.	336.	287.	396.	400.
298.	374.	365.	377.	370.	349.	353.	334.	374.	400.
285.	359.	372.	394.	363.	349.	371.	376.	386.	388.
335.	386.	369.	365.	317.	347.	359.	322.	250.	356.
399.	333.	395.	389.	391.	344.	387.	344.	291.	385.
372.	362.	397.	384.	318.	352.	314.	343.	344.	318.
390.	364.	369.	387.	346.	343.	302.	319.	369.	360.
395.	347.	380.	366.	326.	366.	162.	254.	321.	397.
341.	323.	321.	220.	219.	320.	292.	387.	365.	365.
396.	375.	271.	263.	214.	246.	348.	360.	364.	358.
349.	352.	288.	272.	190.	262.	287.	275.	339.	330.
224.	243.	189.	229.	163.	215.	104.	170.	179.	240.

$$r = \frac{1}{400} \sum_{p=1}^{400} \frac{1}{2} \; (r_{EP} + r_{NP})$$

The symbols r_{EP} and r_{NP} are the peak correlations in the epipolar direction and in the direction normal to the epipolar direction. The average signal power for a block is defined to be

$$S\bar{P} = \frac{1}{400} \sum_{p=1}^{400} 11^* \; \sqrt{\sigma_x^2}$$

The symbol σ_x^2 is the variance of the pixel data from the left image. Note that $\sigma_x 2$ is the generally accepted definition for signal power. The average confidence measure for a block is defined to be

$$C\bar{\phi}N = \frac{1}{400} \sum_{p=1}^{400} C\phi N_p$$

where $C\phi N$ pertains to the Mode 1 match if the match was adjusted successful in Mode 1 or else $C\phi N_p$ pertains to Mode 2. The N_2 values pertain to the total number of successful matches where the success criterion is $C\phi N_p \geq 0.01$.

DISCUSSION. The six topics referred previously are enlarged upon in this section, the topics are:

1. Match Success Parameters
2. Shaping Experiment
3. Array Algebra Experiment
4. General Need for Tuning Test
5. Utilization of Digital Stereo Model
6. Digital Mapping Advantages

The first three topics pertain to the general digital matching procedures used in this report, especially the dependent and independent images. The matching techniques employed for this study are different from the conventional methods used in such devices as UNAMACE, GESTALT, and AS-11-BX in that points to be matched are defined on one image (independent image) rather than defined in a model space. There were two reasons for doing this. The first reason is a practical one in that only one image array need be shaped; whereas, both images must be shaped if the point is defined in a model space. The second reason is that the digital image matching effort at CSL is directed toward an interactive match procedure where it is often necessary to select points for matching from digitized images displayed on a TV screen. The fourth and sixth topics result from the experience gained in the study, and the fifth topic pertains to one of the objectives of the study.

33

Match Success Parameters. A simple scheme was employed in this study to predict whether or not a match was successful. A match was considered successful of $C\phi N \geq 0.01$ where $C\phi N$ is the product of the two second derivatives of the two correlation functions. Further studies should be made to determine whether the average correlation $\bar{r}$, the signal power SP, and the shift in X-parallax PK can be included for a more precise evaluation. A specific combination of $C\phi N$, $\bar{r}$, and PK was used in the K+E study. The graph shown in figure 8 demonstrates the relationship among the three parameters $\bar{r}$, $\overline{SP}$, and N_2 where N_2 is the number of successful matches. The graph pertains to Block 1 through 20 of File 7. File 7 was chosen because it was the subject of the runoff test for shaping versus nonshaping described in the next section and in Appendix B.

It is apparent from the graphs in figure 8 that N_2, the number of successful matches by definition, follows a trend over blocks set out by both $\bar{r}$ and $\overline{SP}$. The signal power, SP, is measured before the match and can therefore be used to predict the likelihood of a successful match or else to select a match strategy. The average correlation value, $\bar{r}$, is measured during the match process and can therefore be used to evaluate the match. For example, the signal power and the average correlation from B13 are low, which should indicate that more work will be required to meet a specific match accuracy for points in the block than those of B5 where the two measures were high.

Note that N_2, the number of successful matches, is larger for B4 than B5, yet $\overline{SP}$ and $\bar{r}$ were lower. When the information content is very high, as in B5, the correlation curve tends to flatten out rather than display a sharp peak. This means that for large values of SP the matching array dimensions should be diminished, or else a more sophisticated shape function should be employed.

Shaping Experiment. Simple first order shaping as described previously in Geometric Description was used in the match process. The purpose of the experiment, described in appendix B and enlarged upon here, was to demonstrate that array shaping is necessary as higher order accuracy requirements are placed on the output. This was done by comparing a nonshaping run to one where the arrays were shaped. One of the rationales for using digital techniques is that complex shaping can be used if necessary; whereas, complex raster shaping in analog methods is impractical. More refined array shaping can be accomplished in several ways. One possible method that offers many advantages is discussed in the next section.

Blocks B2 to B19 of F7 were used in the test. The topography is displayed in figure 2, and the average slope and standard deviation of the slopes are given below in table 8. The average slope is the average of the X-slopes and Y-slopes where all possible slopes were computed for each block. The units in table 8 are degrees.
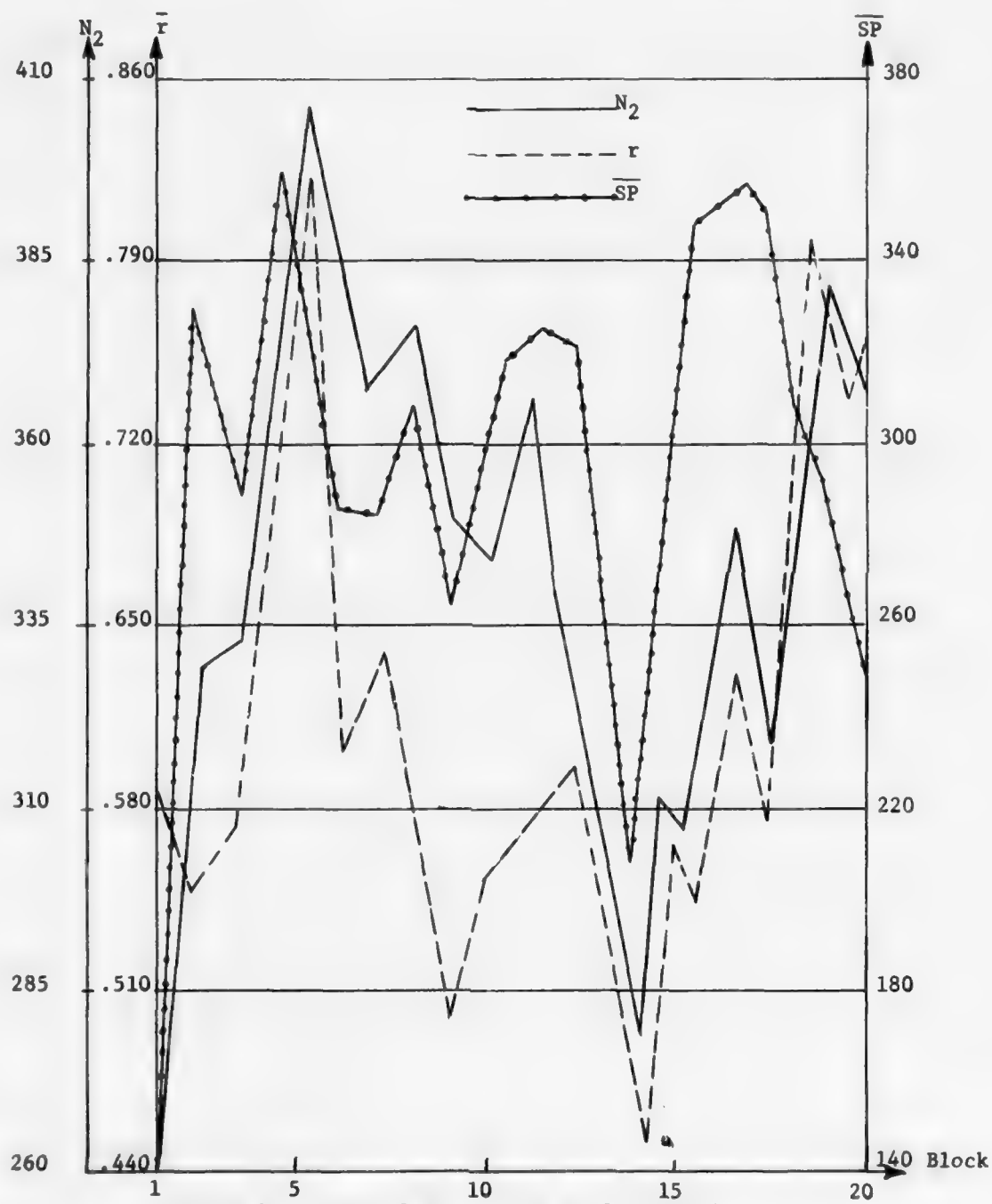
34

Figure 8. Graph of N_2, r, and SP for File 7.

Table 8. Slope Data for File 7.

Block	Slope	Standard Deviation	Block	Slope	Standard Deviation
2	12.2	7.9	11	10.1	6.2
3	13.6	9.5	12	10.7	7.5
4	9.3	4.2	13	13.9	9.7
5	9.2	8.0	14	11.8	5.4
6	11.8	7.5	15	7.3	4.8
7	7.5	5.8	16	4.7	4.1
8	5.5	4.7	17	6.0	4.9
9	8.4	6.2	18	5.2	4.5
10	9.1	5.7	19	4.0	3.4

The graph shown in figure 9 demonstrates the relationship among the three quantities $\overline{SL}$, σ_h, and ΔN_2. The average slope per block, $\overline{SL}$, is taken from table 8; the numerical values for σ_h and ΔN_2 were taken from table B3. The value σ_h is the standard error (in meters) of the difference between the shaping and nonshaping run. The value $\Delta N2$ is the increase in the number of successful matches when the matching arrays are shaped. The graph pertains to Block 2 through 19 of File 7.

It is apparent from the graphs in figure 9 that ΔN_2 and σ_h follow a trend over blocks set out by $\overline{SL}$. As the average slope increases, the standard error in the elevation computation increases. The number of acceptable matches also increases as the average slope increases when the matching arrays are shaped. The results of the experiment demonstrate that array shaping, even the simple method employed in this study, offers a worthwhile improvement in elevation precision and in the number of acceptable matches.

From the observations given in the Preliminary Tests Section, it is apparent that the simple first order shaping employed in this study is only applicable if the array size is small and if the match point spacing is small. Generally, if the match point spacing is large, then the predicted parallax is less accurate, and if the array is large, the first order approximation becomes less realistic. It is also apparent from the results of this section and appendix B that array shaping under the conditions used in this study is effective in computing elevations.

The shaping and predicting process is fundamentally an exercise in extrapolation, which is usually a hazardous operation. This is especially true if the extrapolated points are far removed from the prediction base. The purpose of the correlation process is to verify and refine the prediction. If the extrapolation is over long distances, then the correlation process becomes less realistic.
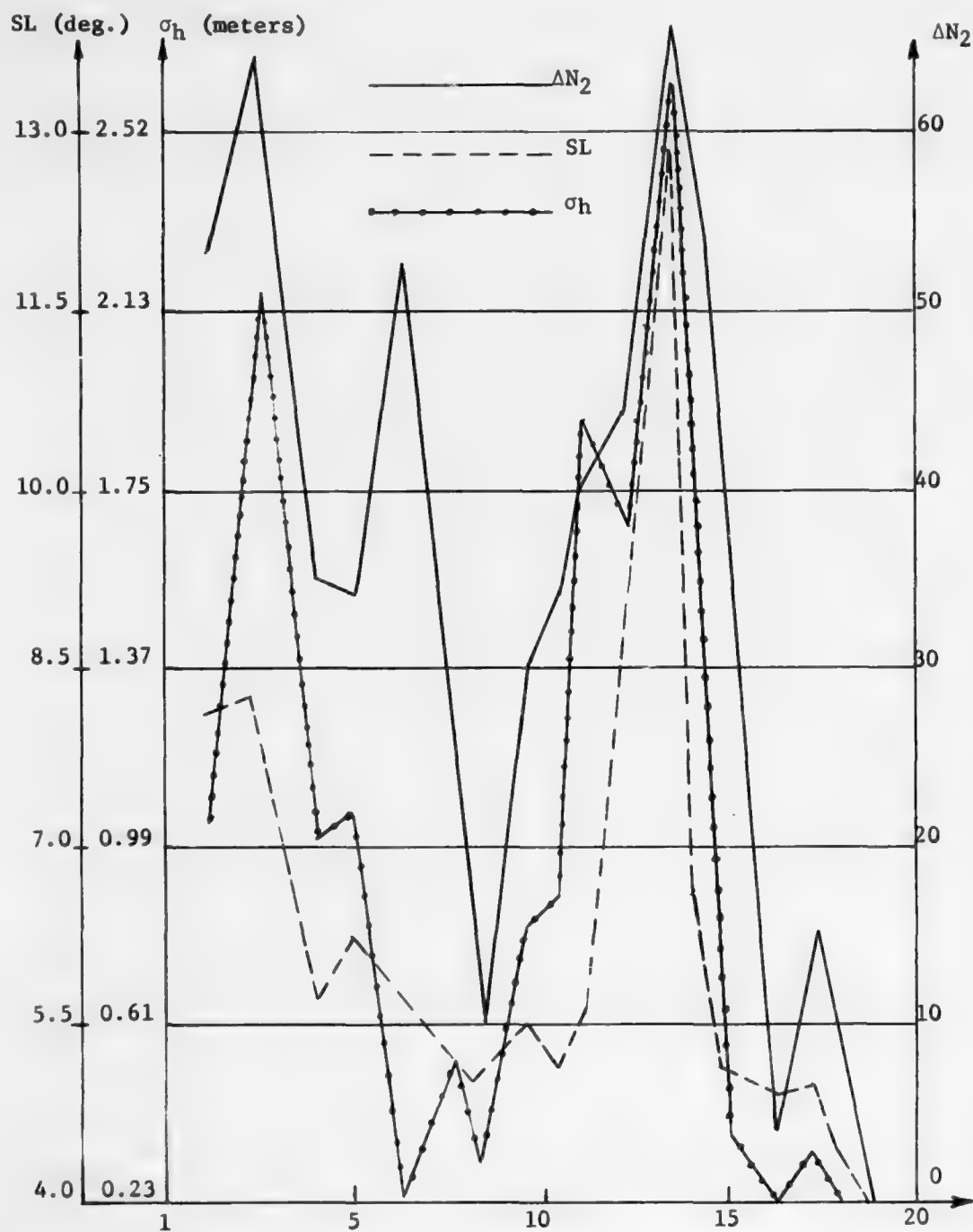
Figure 9. Graph of ΔN_2, $\overline{SL}$, and σ_h For File 7.

37

There are at least three ways to overcome the numerical difficulties described above. The first is to match many points, perhaps more than is needed for the task, such as was done in this study. The second method is to use the basic matching process described in this study but with larger arrays and larger spacings and also to use higher order shaping. The errors in extrapolation still will not go away because the parameters needed for second or higher order shaping must be estimated by differencing parallax data even further removed from the predicted point than was used in first order shaping.

The third method is to concentrate on subregions, wherein points are developed in an iterative fashion over the subregion. The match points are used to develop a warp function, which in turn is used as a predicting point and as a shaping tool. The process is considered complete for a subregion whenever corrections to the predicted points are considered insignificant; the corrections are computed using correlation methods. In this manner, higher order shaping and predicting can be used if a practical means for developing a warp function can be demonstrated. A method for doing this is discussed in the next section.

Array Algebra Experiment. Array algebra[6] as discussed here and in appendix C pertains to the efficient adjustment of one member of the family of multilinear forms, namely the bilinear form. The bilinear form is defined in appendix C as a multiplicative model representation of P X-functions and Q Y-function where the dependent variable is say Z. The model is linear in the P*Q undetermined coefficients and it can be shown that the array algebra solution is identical to the least squares solution.

The number of calculations and required computer storage are far less than for the conventional least squares solution. For example, the solution time for the 256 parameter model discussed in appendix C took about 6 seconds on the CDC-6400 at CSL. Sophisticated coding and better data management could reduce the computer time considerably. The same problem solved in the conventional manner would take over 3 hours.

Such a huge savings in compute power does not occur without constraints on the mensuration exercise. The only constraint, other than linear independence among the unknown coefficients, is that the data must be measured in the XY-frame such that the N X-values and the M Y-values form a regular grid, where $N \geq P$ and $M \geq Q$.

[6] V.A. Rauhala, "New Solutions for Fundamental Colloction and Triangulation Problems," Svensk Lantmateritidskrift 4, Presented in ISP Congress, Comm III, Ottawa.

Five scenes from the digital image shown in figure 2 were selected to aid in the evaluation of the array algebra methods. The five scenes are enlarged and shown again in figure C1. Five bilinear models were defined and fitted to 256 of the 2116 elevation points from each scene. Each scene is about 275 by 275 meters on the ground. One 72-parameter model was defined and used to warp the five dependent image scenes to their corresponding independent scenes. A statistical summary of the terrain roughness for the five scenes is given in table C1. A statistical summary of the image quality and match quality as described in the study is given below. The entries in table 9 were taken from tables 4, 5, 6 and 7.

Table 9. Image and Match Statistics For the Five Scenes

Scene	$S\bar{P}$	$\bar{r}$	$\bar{C\phi N}$	$\bar{N}_2$
1	301	.727	.045	374
2	169	.530	.041	346
3	256	.715	.039	356
4	272	.734	.061	387
5	180	.565	.025	276

The first series of tests were performed to demonstrate how array algebra methods could be used in terrain modelling. The 25 variances associated with the five models for the five scenes are given in table C2. The model standard error is about 1 meter or less for the first four scenes for all five models. The large variances for Scene 5 are attributed to the uncertain matching process caused by the low signal power and high relief. Note that since Model 5 is composed of 256 parameters, the exact number of measurements used in the fit, then the variance estimates are necessarily zero. Residuals were computed for the 1860 points not used in the fit for Model 5. A statistical summary of the fit is given in tables C3 and C4.

The statistical summaries show that the bilinear form can be used successfully in a variety of terrain model exercises. For example, if match points are defined on a grid in model space, then the bilinear model can be used in compilation. If the elevation data is represented by a bilinear form (not necessarily the examples of this study), then its coefficients can be developed in an iterative process where the function itself is used to predict match points and to perform complex image shaping. The function in this case is a terrain model, and contour segments can be developed along with the compilation process and error detection.

The second series of tests were performed to demonstrate how array algebra methods could be used in image warping. A statistical summary of the warp model results is given in table C5. The model standard

error is about 0.7 pixel or less for the first four scenes, and as in the terrain model tests, the standard error for Scene 5 is large for the same reasons as before. A 99 percent confidence interval was constructed, as before, by computing all 2116 residuals.

It is apparent from the statistical summaries that the bilinear form can be used successfully in a variety of image warp operations. For example, if match points are defined on a grid on one image (as was done in this study), then the bilinear form can be used in compilation. If the dependent pixel data is represented by a bilinear form, then its coefficients can be developed in an interactive manner where the function is used for predicting, error detecting, and shaping.

General Need For Tuning Test. A large portion of the effort of this study was directed toward the determination of a practical set of match parameters for the final computer run. The derived set of parameters pertains only to the specific digitized model. If photographic records were collected with a different camera under different taking conditions, then the set of parameters used in this study would not pertain. In fact, if the imagery used for this study were scanned differently (different pixel size and spacing), then again the set of derived parameters would not necessarily pertain.

What is needed is a study to provide operational guidelines for the proper selection of mensuration and matching parameters for successful digital photogrammetric operations on photographic imagery. Photogrammetric operations include pass point selection, target determination, line-of-sight, and other mensuration exercises as well as compilation. The basic problem in computer costs and output accuracies associated with digital photogrammetry is determining practical and accurate means for matching corresponding points on two or more stereo images. This problem pertains whether the operation is an interactive one, as in target determination or map revision, or whether an exotic sensor record is to be compiled on a conventional compilation device. Such a study will provide operational guidelines that will eliminate the usual trial and error methods employed when new imagery is introduced.

There are several obvious sensor record parameters that will tend to characterize the imagery. In photographic imagery, base-height (B/H), scale (H/f), and final image resolution (lp/mm) come immediately to mind. It can be stated that correlation is easiest when B/H = 0 and that it becomes more difficult as B/H increases. On the other hand, elevation accuracy increases as B/H increases; elevations cannot be computed when B/H = 0. It would appear that lp/mm must be considered, especially in relation to B/H. For example, a taking system that produces large values of lp/mm will also produce compilation problems when B/H is large. The type of sensor record, i.e. panoramic, frame, or infrared, will have a great bearing on operating characteristics and achievable accuracies.

Match performance will also be a function of terrain characteristics. Some of the obvious parameters are expected slopes, forest areas, urban areas, featureless areas, occluded areas. Much of this can be monitored somewhat during compilation. For example, signal power is a good indication of image detail. Very low values indicate lack of detail, and large values indicate a busy scene. Image matching tends to become difficult at either extreme.

An analysis of imagery and of the taking parameters, when compared to the output requirements, will provide numerical constraints on the scanner operation and on the match procedure. Scanner characteristics include spot size and shape, spot spacing, signal-to-noise ratio, density accuracy, quantization level, comparator precision. The parameters of match procedure include patch size, match spacing, correlation measure, and a variety of strategies and auxiliary parameters. These include epipolar geometry, scale differences, resolution differences, and image shaping.

Utilization of Digital Stereo Model. One of the objectives of this study was to develop on disc memory at ETL a digitized stereo model complete with a large number of match points, a corresponding set of rectangular local coordinates, and a well-defined relation between the pixel coordinates and the corresponding undistorted photographic coordinates. These results will be used in the following exercises in digital processing:

1. Semi-Automatic Pass Point Mensuration
2. Match Refinement Tests
3. Evaluation of Fourier Matching
4. Image Warp Tests
5. Target Transfer Tests

The pass point work is a continuation of an ETL study on the interactive determination of corresponding points on overlapping digital imagery. The points determined in this study will be used as control for the pass point study, and array algebra methods will be used in areas of high relief. In addition, the derived image control and array algebra methods will be used to perform image warp tests, target transfer tests, and the match refinement tests. The image warp tests will be similar to those performed in this study, and the match refinement tests will be performed over troublesome regions such as Scene 5 described in appendix C. The evaluation of Fourier matching involves converting phase shifts of low frequency harmonics between corresponding digital signals into a linear shift in pixel space.

Digital Mapping Advantages. It became more apparent during the course of the study that digital techniques offer at least three advantages over analog methods; they are:

41

1.   Accuracy
2.   Flexibility
3.   Growth Potential

By utilizing software, output accuracy can range from gross accuracies to the ultimate accuracy that can be extracted from the imagery. The flexibility of the digital computer was emphasized during the preliminary tests where a variety of ideas were examined. Concepts are easy and relatively inexpensive to test in digital computers. It is much easier to discard or modify a poor matching concept when the concept is couched in software than when it is imbedded in hardware. The freedom provided to the analyst by the digital computer in the conceptual design will also provide for increased accuracy. For example, array algebra techniques provide the digital analyst a tool that is denied the analog analyst.

Not only is the capability of growth potential enhanced by the flexibility of software but new computer concepts such as special purpose digital processors and parallel processing can be integrated into existing computer centers more effectively than can they be integrated with analog devices. Studies in digital image processing are being conducted by ETL in these areas. It was shown in an in-house effort that the Goodyear Aerospace Corporation STARAN associative array processor can produce the correlation values needed for matching in times comparable to hardwired devices.[7] A digital cartographic study is being performed at Control Data Corporation to develop a hardware benchmark constructed of special purpose digital processors to determine if the new technology is practical in terms of speed, accuracy, and cost.

Digital image processing will become even more advantageous as mass memories become a reality and as image data is collected digitally. The new computer technologies coupled with mass memories, high speed data rates, solid state array scanners, and new processing techniques such as array algebra will provide image processing capabilities that cannot be achieved by analog methods.

CONCLUSIONS

1. A digital model of a stereo scene of approximately 2,450 by 2,450 square meters was developed and stored on disc at CSL for further studies in digital mapping. The model includes the digitized image pair, 159,600 match points, and their local rectangular coordinates.

2. Digital matching techniques offer accuracy, flexibility, and growth potential capabilities not found in conventional analog methodologies.

7

 David L. Ackerman, Michael A. Crombie and Mary L. Powers Image Correlation on A Parallel Processor. U.S. Army Engineer Topographic Laboratories, Fort Belvoir, VA., ETL-00   April 1976.

42

3. Planning and operating guidance in the proper selection of mensuration and matching parameters is needed for successful digital photogrammetric operations on stereo photographic images.

4. Array algebra methods should be included in any rethinking of digital mapping or digital processing in general.

5. Array shaping is necessary to achieve accurate image correspondence in areas of high relief.

6. Y-parallax errors, if excessive, are easy to monitor and simple to correct using digital techniques.

APPENDIX A. Scale Change For A Straight Line Segment On Vertical
Photography As A Function of Slope

Consider the following diagram. The objective here is to compute the
ratio of the image segments on exposures #1 and #2 that correspond to the
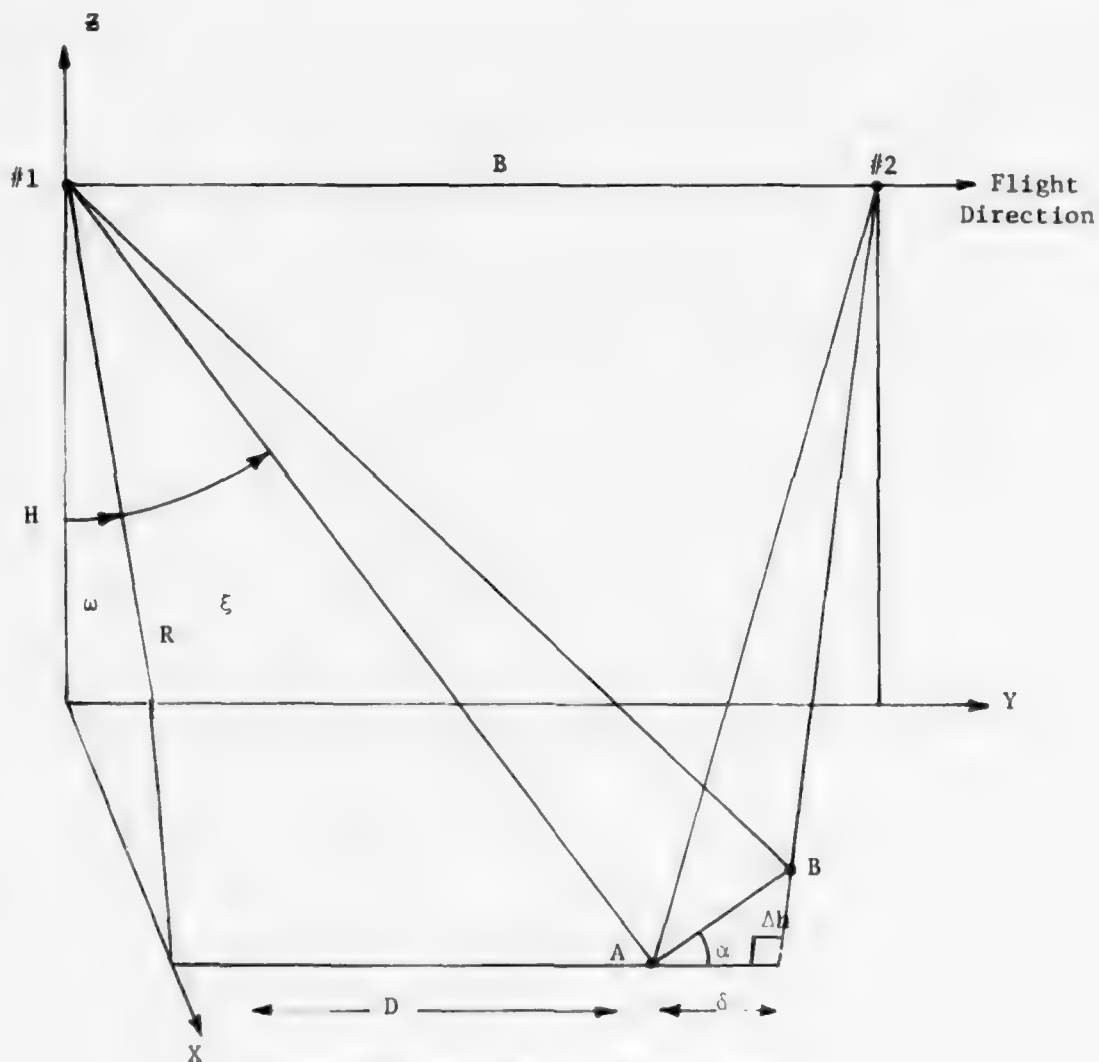ground point segment AB.

Figure A1. Image Segment Geometry.

$$X_A = H \, Tan\omega \qquad X_B = H \, Tan\omega$$

$$Y_A = D \qquad Y_B = D + \delta$$

$$Z_A = 0 \qquad Z_B = h$$

The ratio is simply $S = d_1/d_2$, where d_1 is the image length of the segment AB on #1 and d_2 is the image length of the segment AB on #2.

$$d_1 = \sqrt{(X_{a1} - X_{b1})^2 + (Y_{a1} - Y_{b1})^2}$$

$$d_2 = \sqrt{(X_{a2} - X_{b2})^2 + (Y_{a2} - Y_{b2})^2}$$

The image coordinates are derived directly from the central projection equations, where the two orientation matrices are the identity matrices of order three:

$$X_{a1} = f \, Tan\omega \qquad X_{a2} = f \, Tan\omega$$

$$y_{a1} = \frac{f}{H} D \qquad y_{a2} = \frac{f}{H} (D-B)$$

$$X_{b1} = fH \, Tan\omega/(H-h) \qquad X_{b2} = fH \, Tan\omega/(H-h)$$

$$Y_{b1} = f \, (D + \delta)/(H-h) \qquad y_{b2} = f \, (D + \delta-B)/(H-h)$$

Let
$$\delta = h \cot \alpha$$

and

$$D = H \, Sec \, \omega \, Tan \, \xi$$

Then by direct substitution and after a bit of algebraic simplification

$$d_1 = \frac{fh}{H-h} \, [Tan^2 \, \omega + (Cot \, \alpha + Sec \, \omega \, Tan \, \xi)^2]^{\frac{1}{2}}$$

$$d_2 = \frac{fh}{H-h} \, [Tan^2 \, \omega + (\frac{B}{H} - \cot \, \alpha - Sec \, \omega \, Tan \, \xi)^2]^{\frac{1}{2}}$$

The desired ratio is

$$S = \sqrt{\frac{Tan^2 \omega + (\cot \alpha + Sec \ \omega \ Tan \ \xi)^2}{Tan^2 \ W + (\frac{B}{H} - \cot \alpha - Sec \ \omega \ Tan \ \xi)^2}}$$

The value of S decreases as both ω and ξ increase.

APPENDIX B. Array Shaping Test

The objective of this experiment was to demonstrate the improvement in the match process when simple first order shaping is used compared to nonshaping. Blocks 2 to 19 of File 7 were rerun; wherein, the primary difference between the two runs was that the following shape parameters were used in the second run:

$$U_X = V_Y = 1.0$$

$$U_Y = V_X = 0.0$$

That is, the process was the same in every way except for shaping. In fact, shaping parameters were calculated at each step so that the match point could be estimated more precisely.

The entries in tables B1 and B2 below were extracted directly from the two computer run outputs. The column headings N_1 and N_2 pertain to the number of points successfully matched at the completion of modes 1 and 2 respectively; σ and $\bar{r}$ pertain to the Y-parallax estimates and to the average correlation for the block; and finally $\overline{SP}$ and $\bar{c}$ pertain to the average signal power and average confidence value.

There is little to choose from between the two runs with respect to σ and $\overline{SP}$. In the first case (σ), the apparent equivalence of the Y-parallax errors indicates that ignoring shaping does not introduce Y-parallax error. The signal ($\overline{SP}$) in fact was lower for the shaping run. This is because the process of shaping introduces more dependence among the gray shades, which necessarily reduces the variation and is equivalent to lowering the signal power.

Table B3 lists the differences between the total number of points successfully matched ($\Delta N_2 = N_2 [S] - N_2 [NS]$), the differences between the correlation values ($\Delta r = \bar{r} [S] - \bar{r} [NS]$), and the differences between the confidence values ($\Delta C = \bar{c} [S] - \bar{c} [NS]$). The computer program also produced the average difference (ε) in X-parallax between the two runs for each block and the standard error (σ_ε) for each block. The standard error in X-parallax was converted into a standard error (σ_h in meters) in elevation for each block.

47

Table B1. F7 Results (No Shaping)

Block	N_1	N_2	σ	$\bar{r}$	SP	$\bar{C}$
2	309	353	3.9	.587	214	.043
3	266	295	5.3	.584	223	.029
4	352	379	1.3	.686	312	.039
5	323	358	3.5	.833	381	.041
6	327	351	4.2	.750	282	.035
7	311	341	2.2	.704	234	.034
8	321	356	5.5	.746	261	.032
9	275	325	5.5	.669	182	.029
10	316	351	4.0	.646	205	.032
11	297	328	9.6	.701	219	.030
12	308	332	4.7	.623	233	.032
13	206	239	11.6	.430	155	.021
14	333	364	2.5	.516	224	.039
15	365	393	7.6	.539	211	.059
16	377	392	5.2	.657	259	.066
17	324	369	4.6	.588	225	.043
18	316	362	10.3	.672	355	.042
19	334	356	6.1	.773	315	.047

Table B2. F7 Results (Shaping)

Block	N_1	N_2	σ	$\bar{r}$	$\overline{SP}$	$\bar{C}$
2	307	375	4.2	.636	200	.049
3	310	346	5.3	.647	211	.041
4	376	399	1.4	.752	308	.052
5	336	380	4.0	.859	368	.043
6	327	351	3.9	.793	273	.039
7	312	350	1.3	.736	229	.034
8	312	359	5.5	.754	253	.031
9	287	339	5.6	.690	172	.030
10	324	367	3.9	.682	199	.035
11	314	372	9.8	.732	211	.033
12	329	369	5.1	.657	225	.035
13	251	302	3.6	.485	143	.031
14	348	392	5.4	.584	216	.056
15	367	396	4.4	.565	201	.063
16	374	392	9.8	.688	249	.066
17	313	371	4.4	.607	214	.041
18	317	362	10.5	.685	344	.043
19	334	356	6.0	.784	307	.046

Table B3. Block Differences

Block	ΔN_2	Δr	ΔC	ε	σ_ε	σ_h
2	22	.049	.006	.113	.609	1.25
3	51	.063	.012	.101	.634	1.28
4	20	.066	.013	-.001	.321	0.64
5	22	.026	.002	.111	.398	0.82
6	0	.043	.004	.062	.367	0.73
7	9	.032	.000	-.030	.301	0.61
8	3	.008	-.001	.038	.206	0.43
9	14	.021	.001	-.038	.284	0.58
10	16	.036	.003	.003	.238	0.49
11	44	.031	.003	-.006	.280	0.58
12	37	.034	.003	.109	.467	0.95
13	63	.055	.010	.356	1.230	2.50
14	28	.068	.017	-.009	.443	0.91
15	3	.026	.004	-.025	.244	0.49
16	0	.031	.000	-.038	.213	0.43
17	2	.019	-.002	-.013	.246	0.49
18	0	.013	.001	.022	.170	0.34
19	0	.011	-.001	-.004	.111	0.21

If the results are examined by block and visually compared to File 7 shown on figure 2, then it is apparent that shaping is most effective in steep areas and not particularly effective in the flatter areas. In fact, the shape parameters for perfectly flat areas are exactly those given above. The average X-parallax difference ($\bar{\epsilon}$) turns out to be 0.042 pixels, which is about 1 micrometer. This indicates that ignoring shaping does not introduce an X-parallax bias. The average X-parallax standard error (σ_ϵ) turns out to be 0.450 pixels, which is about 1 meter. This indicates that ignoring shaping does introduce a lack of precision in the elevation determinations. It is expected that the accuracy and precision would diminish even more if the shaping parameters were not used to estimate the match point.

APPENDIX C. Array Algebra Application

Introduction. A specific example of a multilinear form is presented as an example of how array algebra can be used as a tool in digital mapping. The specific form is the bilinear form defined as

$$h\ (X,Y) = f\ (x)\ A\ g^T\ (Y)$$

where

f (X) : (1XP) vector of X-functions

g (Y) : (1XQ) vector of Y-functions

A : (PXQ) array of coefficients

Suppose h (X,Y) is measured at the NXM intersections of the orthonormal grid formed by N X-values and M Y-values. The NXM equations can be organized into the following matrix equation:

$$H = FAG^T$$

where

F: (NXP) array of X-functions

G: (MXQ) array of Y-functions

A: (PXQ) array of coefficients

H: (NXM) array of measurements

The objective of the bilinear solution process is to determine the PXQ coefficients. Assume that $N \geq P$ and that the rank of F is P. Assume also that $M \geq Q$ and the rank of G is Q. Multiply the matrix equation on the left by $\overline{F^T}$ and on the right by G to get

$$F^T\ H\ G = F^T F\ A\ G^T G$$

Multiply this equation on the left by $(F^T F)^{-1}$ and on the right by $(G^T G)^{-1}$ to get the array solution for A.

$$A = (F^T F)^{-1}\ F^T\ HG\ (G^T G)^{-1}$$

This solution is identical to the least squares solution. The array solution involves inverting a PXP matrix and a QXQ matrix; whereas, the least squares solution requires that PQ x PQ matrix be inverted.

Application. A general bilinear form solution was coded in FORTRAN
for the CDC-6400.

$$f(\xi) = [P(\xi), S(\xi), C(\xi)]$$

where

   $P(\xi)$: (1XPZ) vector of powers of ξ

   $S(\xi)$: (1XPS) vector of sine functions of ξ

   $C(\xi)$: (1XPC) vector of cosine function of ξ

The trig functions are multiples of the fundamental period, where the
fundamental period is defined over the range of the ξ-data.

    Data Set. Five data sets were extracted from the set of local
Z-coordinates on disc. Each data set represents approximately a 275 by
275 square-meters area on the ground, or approximately 2.25 blocks by
2.25 blocks. The five scenes can be reviewed on figure 2 of section II.
The northwest block for each of the five scenes is given next, and 5X
enlargements of each scene is presented in figure C1.

    There are a total of 46 by 46 elevations in each set where 256 of
the elevations were used in the bilinear fits. The spacing in each set
is 20 feet (6 meters); whereas, the spacing of the data used in the
bilinear fit is 60 feet (18 meters). A statistical summary of each data
set is given in the following table. The statistics were derived using
all 46 by 46 = 2116 points.

Table C1. Terrain Statistics (in meters)

	Scene				
	1	2	3	4	5
$\bar{h}$	442.7	418.9	375.6	406.3	443.9
σ_h	12.2	16.7	1.9	2.1	17.7
h_{max}	480.9	455.7	386.9	413.6	482.3
h_{min}	421.1	389.1	368.8	401.0	394.0
Range	59.8	66.6	18.1	12.6	88.3

Here, σ_h is regarded as a measure of spread about the mean elevation $\bar{h}$
and not as an error.

53
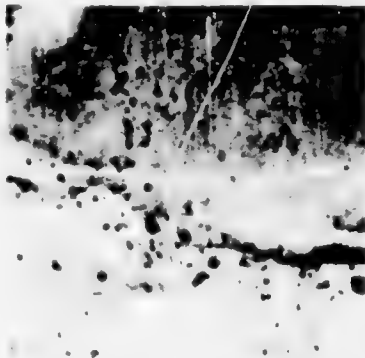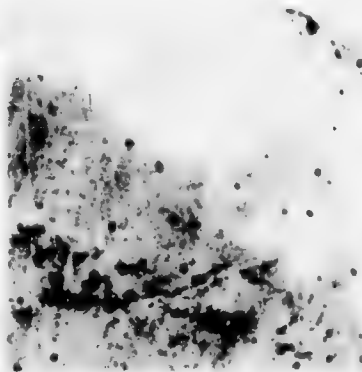
Scene 1 : B3 of F3

Scene 2 : B13 of F7

Scene 3 : B15 of F14
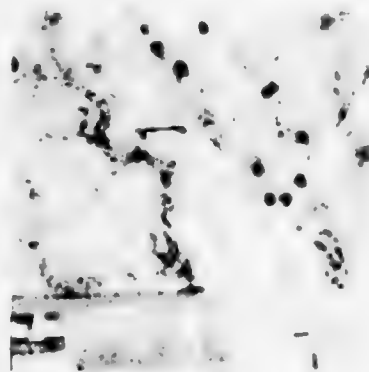
Scene 4 : B3 of F14

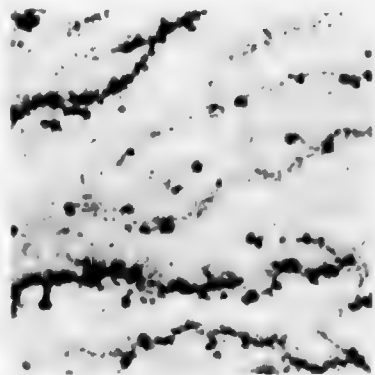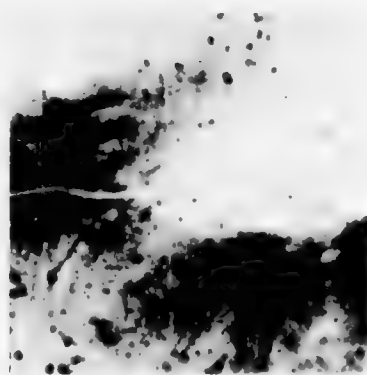Scene 5 : B8 of F12

Scene 1

Scene 2

Scene 3

Scene 4

Scene 5

Figure C1. Test Scenes.

54

Surface Model. The two defining functions f and g were set equal in form for this specific test. An analysis should be made to determine what is the best form for general terrain modeling. Five models (m) were tested in this experiment; note that m=f=g here.

Model 1

$$m(z) = 1, z,$$

Sin Fz, Sin 2Fz, Sin 3Fz, Sin 4Fz,
Cos Fz, Cos 2Fz, Cos 3Fz, Cos 4Fz

$P = Q = 10$; 100 parameters

Model 2

$$m(z) = 1, z, z^2,$$

Sin Fz, Sin 2Fz, Sin 3Fz,
Cos Fz, Cos 2Fz, Cos 3Fz, Cos 4Fz

$P = Q = 10$; 100 parameters

Model 3

$$m(z) = 1, z,$$

Sin Fz, Sin 2Fz, Sin 3Fz, Sin 4Fz, Sin 5Fz,
Cos Fz, Cos 2Fz, Cos 3Fz, Cos 4Fz, Cos 5Fz

$P = Q = 12$; 144 parameters

Model 4

$$m(z) = 1, z,$$

Sin Fz, Sin 2Fz, Sin 3Fz, Sin 4Fz, Sin 5Fz,
Sin 6Fz,

Cos Fz, Cos 2Fz, Cos 3Fz, Cos 4Fz, Cos 5Fz,
Cos 6Fz

$P = Q = 14$; 196 parameters

Model 5

$$m(z) = 1, z,$$

Sin Fz, Sin 2Fz, Sin 3Fz, Sin 4Fz, Sin 5Fz,
                    Sin 6Fz, Sin 7Fz,

                    Cos Fz, Cos 2Fz, Cos 3Fz, Cos 4Fz, Cos 5Fz,
                    Cos 6Fz, Cos 7Fz

          P = Q = 16; 256 parameters

Note that the input data (16 by 16 = 256) satisfied Model 5 exactly;
therefore, the residuals for this model will be exactly zero. Residuals
(for Model 5) were also computed for the (46 by 46 − 16 by 16) = 1,860
points not used in the surface fit.

          Model Error. The program produces the (PxQ) parameter estimates,
the (NxM) residuals, and the model variance estimate.   The variance
estimate is the sum of squares of the residuals divided by the degrees of
freedom. The degrees of freedom value is [(NxM) − (PxQ)]. Only the
model variance estimate is reproduced here.

          Table C2. Terrain Model Error Variances (in square meters)

                                     Scene

Model	1	2	3	4	5
1	1.03	1.15	0.81	0.84	31.18
2	1.10	1.24	0.90	0.73	49.36
3	0.93	1.04	0.70	0.82	31.49
4	0.95	1.15	0.62	0.86	15.92
5	0.00	0.00	0.00	0.00	0.00

The zero model error for Model 5 is because there were as many unknown
parameters (256) as there were equations. In order to determine how well
Model 5 actually represents the data, residuals were computed for the
entire set of 2,116 points.

          Model Error Using Entire Data Set. The objective here is to
see if Model 5 causes large excursions of elevation estimates at points
between the data points used for the fit. The residuals were computed
simply by evaluating the derived function at the 2,116 points. Note that
the 256 points used in the fit will necessarily have zero residuals. A
summary of the errors is given in table C3.

Table 3C. Terrain Model Five Error Summary (in meters)

Scene

	1	2	3	4	5
$\bar{e}$	0.0	0.1	0.1	0.0	-0.6
σ_e	0.88	1.00	1.04	0.78	5.74
e_{max}	3.9	4.3	5.9	3.3	20.5
e_{min}	-7.8	-3.8	-7.3	-4.6	-37.9
Range	11.7	8.1	13.2	7.9	58.4

These data pertain to the 1,860 points not included in the fit.

Cumulative probabilities for the 1,860 residuals were calculated for this example. The cumulative tables represent the distribution of errors over the range of errors. The error range in this example was quantized into 21 equal intervals over the range. Note that the range of errors differs for each scene. The entries in table C4 are probability (prob) $(\epsilon < \xi)$, where ϵ is an error and ξ is the right side of the ξth interval.

Table C4. Terrain Model Five Error Probability Function

Scene

ξ	1	2	3	4	5
1	.0005	.0022	.0005	.0005	.0016
2	.0011	.0054	.0011	.0011	.0027
3	.0011	.0102	.0011	.0011	.0059
4	.0022	.0156	.0016	.0011	.0075
5	.0022	.0312	.0016	.0016	.0129
6	.0027	.0516	.0038	.0038	.0145
7	.0027	.0919	.0051	.0102	.0188
8	.0038	.1737	.0145	.0237	.0280
9	.0078	.3054	.0333	.0629	.0414
10	.0129	.4962	.1016	.1371	.0548
11	.0301	.6753	.2780	.2645	.0699
12	.0720	.8059	.6317	.4812	.1070
13	.2204	.8941	.8397	.6914	.2495
14	.4968	.9371	.9382	.8468	.6774
15	.7935	.9591	.9683	.9258	.8914
16	.9328	.9828	.9866	.9710	.9511
17	.9785	.9941	.9898	.9860	.9763

18	.9919	.9962	.9935	.9919	.9887
19	.9983	.9973	.9957	.9962	.9930
20	.9989	.9984	.9978	.9989	.9962
21	1.0000	1.0000	1.0000	1.0000	1.0000

The cumulative probabilities and the interval definitions can be used to compute confidence intervals for Model 5. For example, 99 percent confidence intervals for the five scenes are

Scene 1: Prob $[-2.8 \leq \varepsilon_1 \leq 2.8] = .99$

Scene 2: Prob $[-3.0 \leq \varepsilon_2 \leq 3.1] = .99$

Scene 3: Prob $[-2.9 \leq \varepsilon_3 \leq 4.6] = .99$

Scene 4: Prob $[-2.7 \leq \varepsilon_4 \leq 2.2] = .99$

Scene 5: Prob $[-29.6 \leq \varepsilon_5 \leq 17.7] = .99$

Consequently, Model 5 represents the terrain quite well for the first four scenes and not well at all for Scene 5.

Discussion. A portion of the error given above is a compilation error, that is errors are introduced into the data set by errors in the matching process. Scene 5 represents a rugged area; wherein, the average correlation was low compared to the other four scenes. Most of the errors occurred at and around the peak in the upper left corner of the scene, an area of low contrast. It is probably more correct to say that the elevation data for Scene 5 needs to be refined than it is to say that the model is deficient.

Utilization of array algebra will then provide the analyst with a means to detect rogue measurements as well as a compaction device. For example, if Model 5 is used, then a reduction of over 8 to 1 is achieved with compaction errors given above. The bilinear model (not necessarily the ones used in this experiment) can be used in compilation. If the elevation data is represented by a bilinear form, then its coefficients can be developed in an iterative process; wherein, the function itself is used to predict matches and to perform complex image shaping. The function in this case is a terrain model and contour segments can be developed along with the compilation process and error detection.

Array algebra techniques can also be used to warp one image to another. If the dependent pixel data is represented by a bilinear form, then its coefficients can be developed in an iterative manner; where as before, the function is used for predicting, error detecting, and shaping.

Image Warp Experiment. A simple test of the image warp capability of array algebra was performed using the corresponding imagery for the five scenes described above. Note that the data was scanned so that the epipolar directions were nearly parallel to the pixel Y-axis. For this reason, the following model was fit to the image points corresponding to the elevation points of the terrain model tests:

$$V\ (X,Y) = f\ (X)\ A\ g^T\ (Y)$$

where

$$f\ (X) = [1,\ X,\ X^2,\ X^3,\ SinF_xX,\ CosF_xX]$$

$$g\ (Y) = [1,\ Y,\ Y^2,\ Y^3,\ SinF_yY,\ Sin2F_yY,\ Sin3F_yY,$$
$$Sin4F_yY,\ CosF_yY,\ Cos2F_yY,\ Cos3F_yY,\ Cos4F_yY]$$

V (X,Y) : Dependent coordinate in epipolar direction

A: (6 x 12) array of unknown coefficients

A summary of the errors is given in table C5; wherein, the units are pixel spacing. The statistical results pertain to all 2,116 points.

Table C5.   Warp Model Error Summary

Scene

	1	2	3	4	5
$\bar{e}$	0.0	0.0	0.0	0.0	-0.2
σ_e	0.62	0.67	0.49	0.46	2.79
e_{max}	2.6	3.2	2.5	2.5	12.2
e_{min}	-4.3	-3.3	-3.3	-2.3	-18.7
Range	6.9	6.5	5.8	4.8	30.9

The cumulative probabilities were computed as before and are presented in table C6.

Table C6. Warp Error Probability Function

Scene

ξ	1	2	3	4	5
1	.0009	.0009	.0009	.0005	.0005
2	.0009	.0019	.0009	.0014	.0024
3	.0014	.0019	.0009	.0019	.0024
4	.0019	.0033	.0028	.0047	.0033
5	.0028	.0090	.0038	.0109	.0071
6	.0052	.0208	.0071	.0265	.0132
7	.0080	.0383	.0113	.0714	.0213
8	.0132	.0846	.0184	.1337	.0312
9	.0250	.1744	.0401	.2698	.0430
10	.0525	.3502	.0912	.4798	.0666
11	.0997	.5836	.2264	.6933	.1224
12	.2164	.7708	.5208	.8549	.2533
13	.4556	.8757	.7717	.9466	.6243
14	.7108	.9291	.9041	.9797	.8549
15	.8842	.9627	.9542	.9896	.9386
16	.9527	.9872	.9853	.9939	.9778
17	.9783	.9943	.9934	.9972	.9915
18	.9929	.9972	.9948	.9989	.9962
19	.9972	.9995	.9953	.9991	.9981
20	.9990	.9995	.9991	.9995	.9991
21	1.0000	1.0000	1.0000	1.0000	1.0000

The cumulative probabilities and the interval definitions can be used to compute confidence intervals for the model above when used as a warp function. For example, 99 percent confidence intervals for the five scenes are

Scene 1: Prob $[-2.0 \leq \epsilon_1 \leq 2.3]$ = .99

Scene 2: Prob $[-1.1 \leq \epsilon_2 \leq 2.6]$ = .99

Scene 3: Prob $[-1.9 \leq \epsilon_3 \leq 1.7]$ = .99

Scene 4: Prob $[-1.4 \leq \epsilon_4 \leq 1.4]$ = .99

Scene 5: Prob $[-11.3 \leq \epsilon_5 \leq 9.3]$ = .99

The units in these intervals are pixels. Just as in the elevation tests, the image warp function does not fit Scene 5 very well.